Pergamon

Int. J. Solids Structures Vol. 35, Nos. 1–2, pp. 149–179, 1998

0020-7683/98 $19.00 + .00

PII: S0020-7683(97)00054-1

CRACK-TIP MICRO MECHANICAL FIELDS IN LAYERED ELASTIC COMPOSITES: CRACK PARALLEL TO THE INTERFACES

M. JHA and P. G. CHARALAMBIDES†
Department of Mechanical Engineering, The University of Maryland, Baltimore County, Baltimore, MD 21228, U.S.A.

(*Received* 12 *August* 1996)

Abstract—Periodically layered bimaterial composites containing cracks parallel to the interfaces at the mid-plane of a layer are considered. The analytical solutions of the plane elastostatic problems under mode-I, mode-II and mixed-mode loading conditions are presented and equations for the crack-tip micro mechanical fields are developed using principles of asymptotic homogenization and the method of complex elastic potentials. An elastic stress singularity of the order $r^{-1/2}$ is shown to exist. The dominating stress intensity factors are found to match with the corresponding values for the equivalent homogeneous orthotropic system. For all cases considered, the stress intensity factors dominating the micro stress field are also defined directly in terms of the stress functions. Comparisons of the analytical results with numerical solutions obtained via refined finite element analyses are presented. Numerical analyses have revealed that the stress field in the immediate vicinity of the crack-tip corresponds to the universal isotropic field dominated by the tip stress intensity factor which depends on the homogenized material properties and those of the layer containing the crack. The effects of micro structural heterogeneity and global anisotropy become predominant beyond the small isotropic region wherein the micro mechanical field is very nicely described by the analytical model. Crack location effects studies are also presented. Implications of the above near-tip fields on delamination fracture in layered systems are discussed. © 1997 Elsevier Science Ltd.

1. INTRODUCTION

The problem of a traction free interface crack located between two bonded isotropic half planes was first studied by several investigators in the early sixties (Erdogan, 1963; England, 1965; Erdogan, 1965; Rice and Sih, 1965). Those solutions exhibited an oscillatory singularity first observed by Williams (1959) and predicted the physically unrealistic phenomenon of material interpenetration and wrinkling of the crack surfaces. Although the presence of an oscillatory singularity in association with a *non-physical* complex stress intensity factor initially hindered further developments in the area of bimaterial fracture, significant progress has been made in recent years (Rice, 1988; Charalambides *et al.*, 1989; Hutchinson and Suo, 1992). A comprehensive overview on these developments are given by Rice (1988) and Hutchinson and Suo (1992). As a logical continuation, the interfacial crack problem between two dissimilar orthotropic half planes was investigated by several researchers (Clements, 1971; Willis, 1971; Ting, 1986; Tewary *et al.*, 1989; Qu and Bassani, 1989; Qu and Bassani, 1993) wherein the oscillatory index was taken into consideration. Defining a physically meaningful stress intensity factor remained a challenge until the late 1980s when Rice (1988) suggested the use of a scale insensitive stress intensity factor. Recently, Qu and Bassani (1989, 1993) developed the necessary and sufficient non-oscillatory conditions and proposed the use of three separate conventional stress intensity factors representing the three classical modes of fracture independently.

The most common approach to deal with the mechanics of heterogeneous media such as wood, laminates, reinforced concrete and some other types of material systems is to treat them as anisotropic homogeneous media and then apply the traditional methods of continuum mechanics. The equations for the crack-tip fields in anisotropic continuum were

† Author to whom correspondence should be addressed.

derived by Sih *et al.* (1965) using the complex variable representation (Muskhelishvili, 1953) wherein an elastic stress singularity of the order $r^{-1/2}$ was shown to exist at the crack-tip. Since the actual micro mechanical heterogeneities are not modeled when using the anisotropic continuum approach, the details of micro failure processes are masked and the actual modes of damage can not be analyzed. For example, the out of plane kinking of a delamination crack has been shown to depend critically on the local conditions at the main crack-tip wherein the mechanics is highly influenced by the immediate material mismatch as measured by the Dundurs parameters (Dundurs, 1969) as well as by the overall geometry of the system, the applied loading, the composite micro structure and material non-linearities. Considerable insight on phenomena such as delamination in layered systems and fiber debonding in fiber reinforced composites has been gained by considering the near-tip mechanics of cracks embedded close to or at the interface in a two layer system. Recent studies (Charalambides, 1991; Zhang, 1994; Ballarini *et al.*, 1995; Jha *et al.*, 1996; Jha and Charalambides, 1996) help expand the family of near-tip solutions in the layered systems by including the effects of the actual layered micro structure on the near-tip mechanics. For example, Charalambides (1991) and later Charalambides *et al.* (1995) developed analytical expressions for the delamination energy release rate made available to the near-tip region associated with a delamination crack embedded in a pre-notched fiber reinforced composite laminate. Those solutions included the effects of an arbitrary combinations of an applied bending moment and applied force which were superimposed on residual thermal and hygroscopic loading. While the above solutions included the salient effects of material orthotropy, lamination and crack morphology as well as finite number of layer effects on the delamination mechanics, they were developed for a specific geometry and did not allow for the evaluation of the actual micro stresses that develop within the K-dominated region surrounding the crack-tip. As discussed by Shaw *et al.* (1993), the knowledge of the actual micro stresses is critical in assessing near-tip non-linearities due to plastic yielding within the ductile layers, brittle matrix damage, crack bridging and crack renucleation and other micro failure phenomena that accompany fracture in layered systems.

In an effort to further our understanding on the near-tip fields in layered systems, Ballarini *et al.* (1995) conducted extensive numerical studies using a *cut-out* heterogeneous layered near-tip zone wherein the elasticity solutions obtained by a remotely applied mode-I loading were obtained via the aid of finite elements. In those studies, Ballarini *et al.* (1995) reported for the first time numerical evidence suggesting the existence of distinct K-dominated zones in the region surrounding the physical crack-tip and in the annular region at radial distance greater than 2 to 3 fiber/matrix unit-cells. The results reported by Ballarini *et al.* (1995) also suggested that the normal micro stress component in the direction parallel to the interfaces may deviate substantially from the averaged unit-cell counterpart which is predicted via homogenization arguments.

Jha *et al.* (1997) expanded the scope of the study by Ballarini *et al.* (1995) by developing an approximate but rather accurate analytical model predicting the near-tip fields first reported by Ballarini *et al.* (1995). Jha *et al.* (1997) also developed an analytical expression relating the tip stress intensity factor to its applied orthotropic counterpart. An alternative and more systematic formulation yielding the mode-I, mode-II and mixed-mode elastic near-tip fields in layered systems containing a crack perpendicular to the interfaces has been recently completed by Jha and Charalambides (1997). In these latter studies, which also include numerical finite element comparisons, the near-tip fields for mode-I, mode-II and mixed-mode were shown to exhibit similar zones of dominance as those first seen by Ballarini *et al.* (1995). The mixed-mode studies conducted by Jha and Charalambides (1997) suggest that either crack shielding or stress intensity amplification that is accompanied by a simultaneous phase shift are induced by the heterogeneous layered micro structure. The phase angle shift is measured as the difference between the mode-mixity dominating the matrix region close to the crack-tip and the remotely applied mode-mixity. The Jha and Charalambides fields are now being used to asses the evolution of small scale plasticity in metal layers adjacent to the crack-tip in brittle/metal stratified composites containing cracks perpendicular to the interfaces.

In this work, a theoretical formulation is developed to describe the micro mechanical crack-tip fields in periodically layered bimaterial systems containing a major crack which is positioned in the middle of a layer and parallel to the interfaces. As in the studies reported by Jha and Charalambides (1997), the effects of the periodic micro structure are introduced in the solution through an asymptotic homogenization method (Bensoussan *et al.*, 1978; Sanchez-Palencia, 1980; Christensen, 1991). As shown in these homogenization studies, the higher order terms in the asymptotic expansion of the displacement field utilize the successive gradients of the macroscopic strains as well as other tensor characteristics of the micro structure. When retaining such higher order terms, the ensuing model incorporates highly non-linear non-local effects induced by the heterogeneous micro structure. The resulting macroscopic description of the problem is solved using the method of complex elastic potentials (Lekhnitskii, 1963; Muskhelishvili, 1953). For problems involving lines of discontinuities, the complex elastic potentials are sectionally holomorphic (Muskhelishvili, 1953) and their representation close to the crack-tip are available in the literature and will be used in this work.

The structure of this paper is as follows. The basic formulation of the asymptotic homogenization for the two dimensional plane strain problem is presented in Section 2. The crack-tip micro stress fields for a crack parallel to the interfaces and running through the mid-plane of a layer are also derived in Section 2. In addition to the analytical formulation, near-tip finite element studies were also performed within a heterogeneous *cut-out* region surrounding the physical crack-tip which are presented in Section 3. Sample analytical calculations and corresponding numerical results are presented in Section 4. Section 5 features numerical studies on the effects of crack location on the delamination mechanics. The concluding remarks are presented in Section 6.

2. PROBLEM STATEMENT

Consider the wide thickness layered specimens shown in Fig. 1, of length $2C$, height $2h$ and thickness w. As shown in the above figure, each of the specimens contains a delamination crack of length a. In order to preserve material and geometric symmetry as required for the case of pure mode-I and pure mode-II, the delamination crack plane will be taken to coincide with the mid-plane of the mode-I and the mode-II specimens shown in Figs 1a and 1b, respectively. The layered geometry shown in Fig. 1c however, as discussed elsewhere (Zhang, 1994), is inherently subjected to near-tip mixed-mode conditions. Such conditions may also arise for geometries and loading similar to those shown in Figs 1a and 1b whenever they contain delamination cracks positioned away from the mid-plane of the specimen.

A lamination micro structure comprising of alternating soft matrix and stiff fiber layers will be considered. With the exception of the systems considered in Section 5 of this work where the crack location effects are studied, and for reasons similar to those used by Jha *et al.* (1997) and Jha and Charalambides (1997), the delamination crack will be placed in the middle of a layer, but unlike the systems considered in previous work, in this study the crack plane will be considered to be parallel to the interfaces.

2.1. *Asymptotic homogenization and stress-strain relations*

For each of the systems shown in Fig. 1, consider now a *cut-out* region containing the crack-tip as shown in Fig. 2. For the purpose of this study, we shall consider that a sufficient number of layers exists over the length R of the *cut-out* region such that outside this region homogenization arguments can be applied. In the general case of mixed-mode loading, the near-tip orthotropic displacements can be applied at the *cut-out* boundary provided that R is sufficiently smaller compared to a macroscopic specimen dimension such as the height h. Under these conditions, we shall seek the elasticity solution for the displacement, strain and stress fields dominating the near tip *cut-out* region shown in Fig. 2.

Within the well established framework of asymptotic homogenization technique (Bensoussan *et al.* (1978)), the micro-displacements for the periodically layered system in the absence of the crack can be considered as a two space variable $\mathbf{u}(\mathbf{x}, \xi)$ where $\xi = x_2/\epsilon$ is

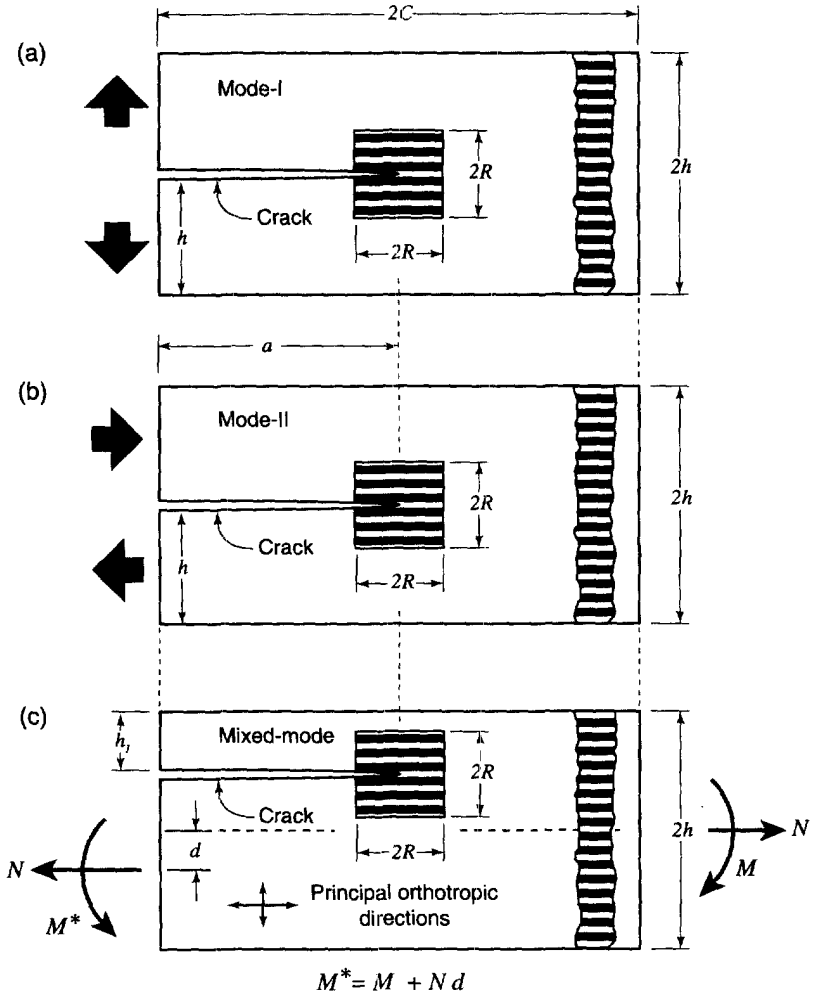

Fig. 1. Schematic diagrams of periodically layered bimaterial specimens with a major crack embedded parallel to the interfaces.

the fast scale variable and $\epsilon = l/R$ represents the ratio of the micro structural length l to the characteristic macro length R and is assumed to be small. Thus, the displacements can be expressed as an asymptotic expansion in terms of the homogenized displacement $\mathbf{u}^0(\mathbf{x})$ and the asymptotic parameter ϵ such that:

$$u_i(\mathbf{x}, \xi) = u_i^0(\mathbf{x}) + \epsilon U_{ij}(\xi)\bar{\varepsilon}_j^0(\mathbf{x}) + \cdots \tag{1}$$

where $\bar{\varepsilon}_j^0(\mathbf{x})$ are the averaged strain components corresponding to the mean zero order displacements $\mathbf{u}^0(\mathbf{x})$. In the above expression, the strains are represented using the standard contracted notation. The unknown functions $U_{ij}(\xi)$ in eqn (1) are to be obtained by solving the local equations of elastostatics with the indices taking on values $i = 1, 2$ and $j = 1, 2$ and 6. The above form of asymptotic displacement expansion and other aspects of homogenization in periodically layered systems are presented in most detail in the paper by Jha and Charalambides (1996). The zero order infinitesimal micro-strains after neglecting higher order terms are given by:

$$\begin{Bmatrix} \varepsilon_1 \\ \varepsilon_2 \\ \varepsilon_6 \end{Bmatrix} = \begin{pmatrix} 1 & 0 & 0 \\ U_{21,\xi} & 1+U_{22,\xi} & U_{26,\xi} \\ U_{11,\xi} & U_{12,\xi} & 1+U_{16,\xi} \end{pmatrix} \begin{Bmatrix} \bar{\varepsilon}_1^0 \\ \bar{\varepsilon}_2^0 \\ \bar{\varepsilon}_6^0 \end{Bmatrix} \tag{2}$$

where $(,\xi)$ implies partial derivative with respect to the fast scale variable $\xi = x_2/\epsilon$. Under

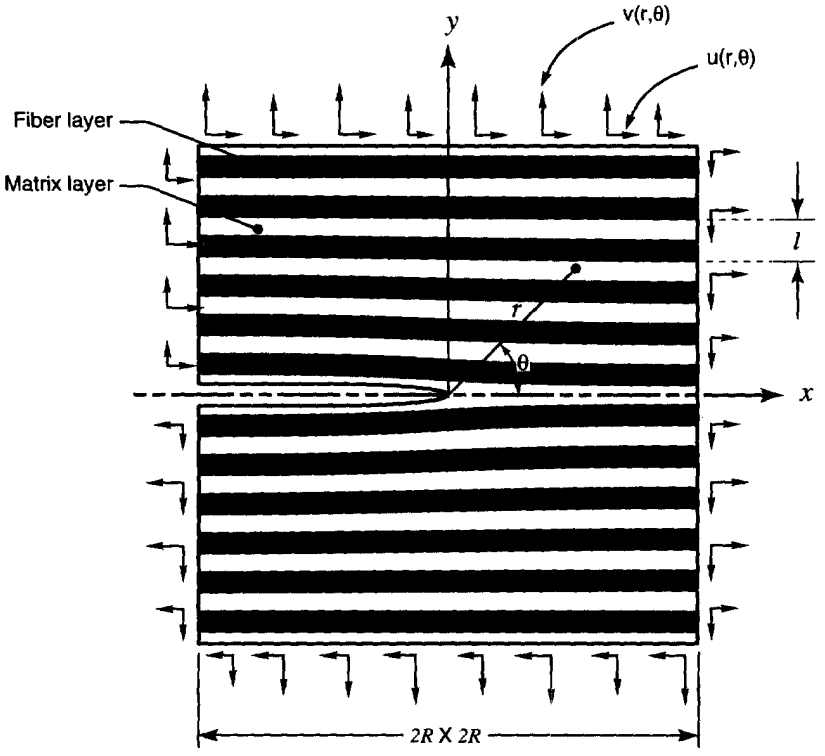

Fig. 2. The near-tip plane strain boundary value problem used in the finite element studies.

plane strain conditions, the micro stresses at any point in the unit-cell are obtained using the local constitutive relations such that the local stress-strain relations take the following form:

$$\begin{Bmatrix}\sigma_1\\ \sigma_2\\ \sigma_6\end{Bmatrix} = \begin{pmatrix} C'_{11} & C'_{12} & C'_{16}\\ C'_{21} & C'_{22} & C'_{26}\\ C'_{61} & C'_{62} & C'_{66}\end{pmatrix}\begin{Bmatrix}\bar{\varepsilon}_1^0\\ \bar{\varepsilon}_2^0\\ \bar{\varepsilon}_6^0\end{Bmatrix} \tag{3}$$

where $C'_{ij}(\xi)$ are the effective local stiffnesses given by:

$$\begin{aligned}
C'_{11} &= C_{11} + C_{12}U_{21,\xi}\\
C'_{12} &= C_{12} + C_{12}U_{22,\xi}\\
C'_{16} &= C_{12}U_{26,\xi}\\
C'_{21} &= C_{12} + C_{22}U_{21,\xi}\\
C'_{22} &= C_{22} + C_{22}U_{22,\xi}\\
C'_{26} &= C_{22}U_{26,\xi}\\
C'_{61} &= C_{66}U_{11,\xi}\\
C'_{62} &= C_{66}U_{12,\xi}\\
C'_{66} &= C_{66} + C_{66}U_{16,\xi}
\end{aligned} \tag{4}$$

and C_{ij} $(i = j = 1, 2, 6)$ are the elastic moduli of the lamina at the point of interest.

Noting that the effective local elastic moduli C'_{ij} are functions of ξ only and after neglecting higher order terms, the local elastostatic equilibrium in the absence of body forces yields:

$$\frac{\partial C'_{21}}{\partial \xi}\bar{\varepsilon}_1^0 + \frac{\partial C'_{22}}{\partial \xi}\bar{\varepsilon}_2^0 + \frac{\partial C'_{26}}{\partial \xi}\bar{\varepsilon}_6^0 = 0$$

$$\frac{\partial C'_{61}}{\partial \xi}\bar{\varepsilon}_1^0 + \frac{\partial C'_{62}}{\partial \xi}\bar{\varepsilon}_2^0 + \frac{\partial C'_{66}}{\partial \xi}\bar{\varepsilon}_6^0 = 0. \tag{5}$$

Since the above equations are to be satisfied for all values of $\bar{\varepsilon}_i^0$, $i = 1, 2, 6$; the following must hold within each unit-cell (see Fig. 3):

$$\frac{\partial}{\partial \xi}\left(C_{12} + C_{22}\frac{\partial U_{21}}{\partial \xi}\right) = 0$$

$$\frac{\partial}{\partial \xi}\left(C_{22} + C_{22}\frac{\partial U_{22}}{\partial \xi}\right) = 0$$

$$\frac{\partial}{\partial \xi}\left(C_{22}\frac{\partial U_{26}}{\partial \xi}\right) = 0$$

$$\frac{\partial}{\partial \xi}\left(C_{66}\frac{\partial U_{11}}{\partial \xi}\right) = 0$$

$$\frac{\partial}{\partial \xi}\left(C_{66}\frac{\partial U_{12}}{\partial \xi}\right) = 0$$

$$\frac{\partial}{\partial \xi}\left(C_{66} + C_{66}\frac{\partial U_{16}}{\partial \xi}\right) = 0. \tag{6}$$

Moreover, the continuity of the displacements and the traction should be maintained at the matrix/fiber interfaces. Denoting the jump in the field quantities across the interface, i.e. the difference between the values of a discontinuous quantity directly ahead of and immediately behind the interface as $[\![\cdot]\!]$, the displacement and the tractions continuity respectively can be expressed as:

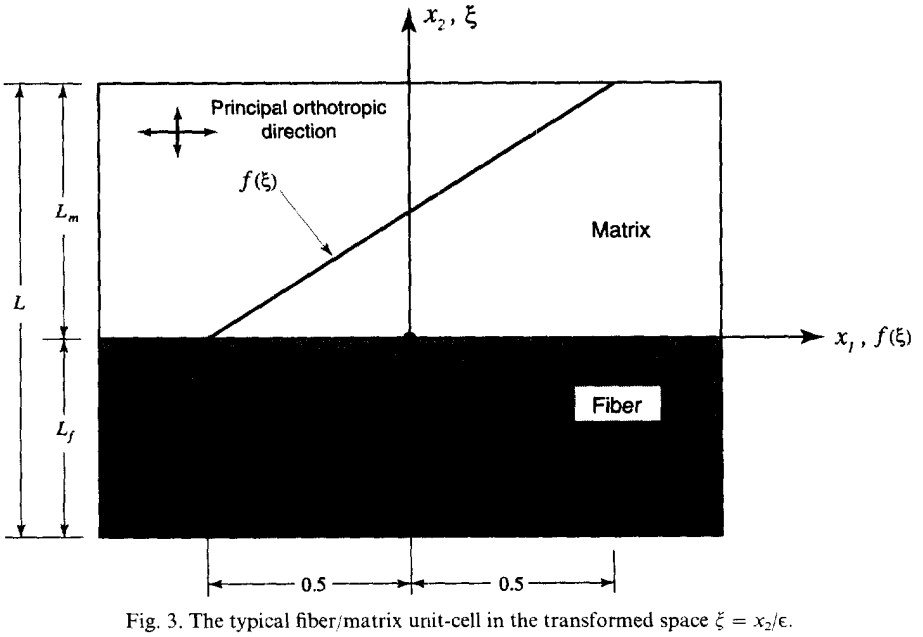

Fig. 3. The typical fiber/matrix unit-cell in the transformed space $\xi = x_2/\epsilon$.

$$[\![u_i]\!] = 0 \quad \text{for displacement continuity} \tag{7}$$

and

$$[\![\sigma_{ij}N_i]\!] = 0 \quad \text{for traction continuity} \tag{8}$$

where N_i are the components of the unit normal to the matrix/fiber interface. The above continuity conditions require, in turn, that the unknown functions U_{ij} must satisfy the following conditions:

$$[\![U_{ij}]\!] = 0 \tag{9}$$

and

$$[\![C'_{ijmn}N_i]\!] = 0. \tag{10}$$

The solution to the local equilibrium eqn (6) subject to the continuity conditions (9) and (10) yields the periodic functions $U_{ij}(\xi)$. As can be seen, the equilibrium eqns (6) are all of the following type:

$$\partial[\alpha \cdot \partial(U)/\partial\xi + \beta]/\partial\xi = 0 \tag{11}$$

where α and β represent material constants which are piece-wise smooth and L-periodic on the fast scale ξ. The general solution of the above equation, satisfying the continuity conditions (7)–(8) at the interfaces, is the continuous L-periodic function U given by [Boutin (1996)]:

$$U(\xi) = f(\xi) \cdot \langle \alpha^{-1} \rangle^{-1} \mathbf{D}(\alpha^{-1})\mathbf{D}(\beta)/\mathbf{D}(\alpha) \tag{12}$$

where, by convention, for each piecewise continuous function φ taking the constant values φ_m and φ_f in the matrix and the fiber layer, respectively, the following notation has been used:

$$\mathbf{D}(\varphi) = v_f v_m L(\varphi_m - \varphi_f) \tag{13}$$

with v_f and v_m representing the fiber and matrix volume fractions, respectively. Also in eqn (12), the shape function $f(\xi)$ is given by:

$$f(\xi) = \begin{cases} \dfrac{\xi}{L_m} - \dfrac{1}{2} & \text{in the matrix layer} \\ -\dfrac{\xi}{L_f} - \dfrac{1}{2} & \text{in the fiber layer} \end{cases}. \tag{14}$$

The profile of $f(\xi)$ within the fiber/matrix unit-cell along the fast scale ξ is shown in Fig. 3. Note that $L = L_f + L_m$ represents the unit-cell thickness on the fast scale ξ while the thickness of the same unit-cell on the **x**-scale is taken to be $l = l_m + l_f$ as shown in Fig. 2. Thus, the solution of the local equilibrium yields the following expressions for the unknown functions U_{ij}:

$$\begin{aligned} U_{22} &= f(\xi) \cdot \langle C_{22}^{-1} \rangle^{-1} \mathbf{D}(C_{22}^{-1}) \\ U_{21} &= f(\xi) \cdot \langle C_{22}^{-1} \rangle^{-1} \mathbf{D}(C_{22}^{-1})\mathbf{D}(C_{12})/\mathbf{D}(C_{22}) \\ U_{16} &= f(\xi) \cdot \langle C_{66}^{-1} \rangle^{-1} \mathbf{D}(C_{66}^{-1}) \\ U_{26} &= U_{12} = U_{11} = 0. \end{aligned} \tag{15}$$

The effective local elastic moduli associated with the macroscopic strain $\bar{\varepsilon}_i^0$ can now be obtained with the help of eqns (4) and (15) as:

$$
\begin{aligned}
C'_{22} &= 1/\langle 1/C_{22}\rangle \\
C'_{21} &= \langle C_{12}/C_{22}\rangle/\langle 1/C_{22}\rangle \\
C'_{12} &= \frac{C_{12}}{C_{22}}/\langle 1/C_{11}\rangle \\
C'_{11} &= C_{11}+\frac{C_{12}}{C_{22}}(C'_{21}-C_{12}) \\
C'_{66} &= 1/\langle 1/C_{66}\rangle \\
C'_{16} &= C'_{26} = C'_{61} = C'_{62} = 0.
\end{aligned} \tag{16}
$$

The macroscopic elastic moduli are obtained by averaging the above moduli over the unit-cell volume. For the planar case we obtain the macroscopic elastic moduli as:

$$
\begin{aligned}
C^0_{11} &= \langle C_{11}-C_{12}C_{12}/C_{22}\rangle+\langle C_{12}/C_{22}\rangle^2/\langle 1/C_{22}\rangle \\
C^0_{22} &= 1/\langle 1/C_{22}\rangle \\
C^0_{12} &= C^0_{21} = \langle C_{12}/C_{22}\rangle/\langle 1/C_{22}\rangle \\
C^0_{66} &= 1/\langle 1/C_{66}\rangle \\
C^0_{16} &= C^0_{26} = C^0_{61} = C^0_{62} = 0.
\end{aligned} \tag{17}
$$

It is evident from eqns (16) and (17) that some of the effective local elastic coefficients are equal to the respective overall elastic coefficients for the homogenized medium. Making use of this resemblance, the micro stresses in the layered system can be expressed as:

$$
\begin{aligned}
\sigma_{xx} &= \left[C_{11}+\frac{C_{12}}{C_{22}}(C^0_{12}-C_{12})\right]\bar{\varepsilon}^0_{xx}+\frac{C_{12}}{C_{22}}C^0_{22}\bar{\varepsilon}^0_{yy} \\
\sigma_{yy} &= C^0_{12}\bar{\varepsilon}^0_{xx}+C^0_{22}\bar{\varepsilon}^0_{yy} \\
\sigma_{xy} &= C^0_{66}\bar{\gamma}^0_{xy}
\end{aligned} \tag{18}
$$

where C_{ij} $(i,j = 1,2,6)$ are the local stiffnesses and C^0_{ij} $(i,j = 1,2,6)$ are the stiffnesses of the homogenized medium. The double subscript notation for the stresses and the strains in eqn (18) has been used merely for convenience and will be followed hereafter.

2.2. *Crack-tip micro stress fields*

We will seek here the approximate analytical solutions for the deformation and stress fields in the near-tip region shown in Fig. 2 of a semi-infinite crack embedded parallel to the interfaces in a layered system. As depicted in Fig. 2 the crack-plane is assumed to be located in the mid-plane of the matrix layer, with no traction acting on the crack surfaces. The zero-order homogenized displacements will be taken as the general expressions for the plane deformation of the anisotropic continuum using the appropriate complex elastic potentials (Lekhnitskii, 1963). With the aid of the strain displacement relations and eqn (18), the equations for the micro stresses in the layered systems under consideration will be then obtained in terms of the same complex elastic potentials. By choosing these potential functions to be the holomorphic functions representing the crack-tip fields in the homogeneous domain, the zero order mode-I and mode-II micro stress fields dominating the crack-tip region of a crack embedded in a layered system (See Figs 1 and 2) will be derived. The analysis shall be presented next in detail.

For anisotropic materials, the generalized Hooke's law in contracted notation is given by:

$$\varepsilon_i = S_{ij}\sigma_j \quad i,j = 1,2,\ldots,6 \tag{19}$$

where $[S_{ij}] = [S_{ji}]$ is the compliance matrix for the material. When the material has a plane of elastic symmetry normal to the z-axis, the Hooke's law for the deformation in the (x, y) plane (Lekhnitskii, 1963) reduces to:

$$\varepsilon_i = b_{ij}\sigma_j \quad i,j = 1,2,6$$
$$b_{ij} = \begin{cases} S_{ij} & \text{for plane stress} \\ S_{ij} - \dfrac{S_{i3}S_{j3}}{S_{33}} & \text{for plane strain} \end{cases} \tag{20}$$

It has been shown in Likhnitskii (1963) that the problems of plane anisotropic elasticity can be conveniently formulated in terms of two analytic functions, $\phi_1(z_1)$ and $\phi_2(z_2)$ with two complex variables $z_1 = x+\mu_1 y$ and $z_2 = x+\mu_2 y$. The parameters μ_1 and μ_2 are the roots of the characteristic equation:

$$b_{11}\mu^4 - 2b_{16}\mu^3 + (2b_{12}+b_{66})\mu^2 - 2b_{26}\mu + b_{22} = 0. \tag{21}$$

The roots of eqn (21) are always complex and occur in conjugate pairs. In forming the complex variables z_j, μ_1 and μ_2 are chosen as those with positive imaginary parts. The displacements for the homogeneous anisotropic continuum are given by:

$$u = 2\,\mathrm{Re}\,[p_1\phi_1(z_1) + p_2\phi_2(z_2)]$$
$$v = 2\,\mathrm{Re}\,[q_1\phi_1(z_1) + q_2\phi_2(z_2)] \tag{22}$$

where $\mathrm{Re}\,[\cdot]$ signifies the real part of a complex number, and

$$p_j = b_{11}\mu_j^2 + b_{12} - b_{16}\mu_j$$
$$q_j = b_{12}\mu_j + b_{22}/\mu_j - b_{26}. \tag{23}$$

The global solution of the anisotropic continuum obtained by the homogenization of the layered system will be sought using the above method of complex elastic potentials. The compliances of the homogenized domain will be taken as $[S_{ij}] = [C_{ij}^0]^{-1}$ and the zero order mean strain will be constructed from the symmetric gradients of the mean displacements for the anisotropic continuum. Thus, using the expressions for the displacements given above, the zero-order mean strains are obtained as:

$$\bar{\varepsilon}_{xx}^0 = 2\,\mathrm{Re}\,[p_1\phi_1'(z_1) + p_2\phi_2'(z_2)]$$
$$\bar{\varepsilon}_{yy}^0 = 2\mathrm{Re}\,[q_1\mu_1\phi_1'(z_1) + (Q_2\mu_2\phi_2'(z_2)]$$
$$\bar{\gamma}_{xy}^0 = 2\mathrm{Re}\,[(p_1\mu_1 + q_1)\phi_1'(z_1) + (p_2\mu_2 + q_2)\phi_2'(z_2)]. \tag{24}$$

With the aid of eqns (18) and (24), the zero-order micro stresses take the form:

$$\sigma_{xx} = 2\,\mathrm{Re}\,[\mu_1^*\phi_1'(z_1) + \mu_2^*\phi_2'(z_2)]$$
$$\sigma_{yy} = 2\,\mathrm{Re}\,[\phi_1'(z_1) + \phi_2'(z_2)]$$
$$\sigma_{xy} = -2\,\mathrm{Re}\,[\mu_1\phi_1'(z_1) + \mu_2\phi_2'(z_2)] \tag{25}$$

where

$$\mu_1^* = \frac{C_{12}}{C_{11}} + p_1\left(C_{11} - \frac{C_{12}^2}{C_{22}}\right)$$

$$\mu_2^* = \frac{C_{12}}{C_{11}} + p_2\left(C_{11} - \frac{C_{12}^2}{C_{22}}\right). \tag{26}$$

From eqns (26), it is evident that μ_1^* and μ_2^* are functions of $\xi = x_2/\epsilon$ and are discontinuous at the fiber/matrix interfaces. As a result, the stress component σ_{xx} will also exhibit a discontinuity at all interfaces while σ_{yy} and σ_{xy} which do not depend on μ_1^* and μ_2^* remain continuous spatial functions. As discussed earlier, the functions $\phi_1(z_1)$ and $\phi_2(z_2)$ will be those functions associated with the elasticity solution for an anisotropic body containing a macro-crack. For an infinite body containing a semi-infinite crack, the holomorphic stress functions $\phi_1(z_1)$ and $\phi_2(z_2)$ [Muskhelishvili (1953)] associated with the elastic asymptotic solution near the crack-tip may be approximated by (Sih *et al.*, 1965):

$$\phi_1'(z_1) = \frac{\lambda_{10}}{\sqrt{r(\cos\theta + \mu_1 \sin\theta)}}$$

$$\phi_2'(z_2) = \frac{\lambda_{20}}{\sqrt{r(\cos\theta + \mu_2 \sin\theta)}} \tag{27}$$

where λ_{10} and λ_{20} are complex coefficients. Thus, in light of the above equations and the aid of eqn (25), the near-tip micro stresses take the form:

$$\sigma_{xx} = 2\,\mathrm{Re}\left[\frac{\mu_1^*\lambda_{10}}{\sqrt{r(\cos\theta + \mu_1 \sin\theta)}} + \frac{\mu_2^*\lambda_{20}}{\sqrt{r(\cos\theta + \mu_2 \sin\theta)}}\right]$$

$$\sigma_{yy} = 2\,\mathrm{Re}\left[\frac{\lambda_{10}}{\sqrt{r(\cos\theta + \mu_1 \sin\theta)}} + \frac{\lambda_{20}}{\sqrt{r(\cos\theta + \mu_2 \sin\theta)}}\right]$$

$$\sigma_{xy} = -2\,\mathrm{Re}\left[\frac{\mu_1\lambda_{10}}{\sqrt{r(\cos\theta + \mu_1 \sin\theta)}} + \frac{\mu_2\lambda_{20}}{\sqrt{r(\cos\theta + \mu_2 \sin\theta)}}\right]. \tag{28}$$

Following the standard definition of the mode-I and mode-II stress intensity factors, K_I and K_II are given as:

$$K_\mathrm{I} = \lim_{r\to 0} \sqrt{2\pi r}\, \sigma_{yy}(r, 0) \tag{29}$$

$$K_\mathrm{II} = \lim_{r\to 0} \sqrt{2\pi r}\, \sigma_{xy}(r, 0). \tag{30}$$

The above equations when combined with the stress equations given by (28) yield the stress intensity factors K_I and K_II in terms of the complex constants λ_{10} and λ_{20} as follows:

$$K_\mathrm{I} = 2\sqrt{2\pi}\,\mathrm{Re}\,[\lambda_{10} + \lambda_{20}] \tag{31}$$

$$K_\mathrm{II} = -2\sqrt{2\pi}\,\mathrm{Re}\,[\mu_1\lambda_{10} + \mu_2\lambda_{20}]. \tag{32}$$

By redefining λ_{10} and λ_{20} in terms of K_I and K_II as:

$$\lambda_{10} = \frac{1}{2\sqrt{2\pi(\mu_1 - \mu_2)}}[\mu_2 K_I + K_{II}] \tag{33}$$

$$\lambda_{20} = \frac{-1}{2\sqrt{2\pi(\mu_1 - \mu_2)}}[\mu_1 K_I + K_{II}] \tag{34}$$

the micro stresses in the matrix and the fiber phases for Mode-I loading are given by the following classical expressions:

Mode-I micro stresses:

$$\begin{aligned}
\sigma_{xx}^{(m)} &= \frac{K_I}{\sqrt{2\pi r}} \operatorname{Re}\left[\frac{1}{(\mu_1 - \mu_2)}\left(\frac{\mu_1 \mu_2^{*(m)}}{\sqrt{\cos\theta + \mu_2 \sin\theta}} - \frac{\mu_2 \mu_1^{*(m)}}{\sqrt{\cos\theta + \mu_1 \sin\theta}}\right)\right] \\
\sigma_{yy}^{(m)} &= \frac{K_I}{\sqrt{2\pi r}} \operatorname{Re}\left[\frac{1}{(\mu_1 - \mu_2)}\left(\frac{\mu_1}{\sqrt{\cos\theta + \mu_2 \sin\theta}} - \frac{\mu_2}{\sqrt{\cos\theta + \mu_1 \sin\theta}}\right)\right] \\
\sigma_{xy}^{(m)} &= \frac{K_I}{\sqrt{2\pi r}} \operatorname{Re}\left[\frac{\mu_1 \mu_2}{(\mu_1 - \mu_2)}\left(\frac{1}{\sqrt{\cos\theta + \mu_1 \sin\theta}} - \frac{1}{\sqrt{\cos\theta + \mu_2 \sin\theta}}\right)\right]
\end{aligned} \tag{35}$$

$$\begin{aligned}
\sigma_{xx}^{(f)} &= \frac{K_I}{\sqrt{2\pi r}} \operatorname{Re}\left[\frac{1}{(\mu_1 - \mu_2)}\left(\frac{\mu_1 \mu_2^{*(f)}}{\sqrt{\cos\theta + \mu_2 \sin\theta}} - \frac{\mu_2 \mu_1^{*(f)}}{\sqrt{\cos\theta + \mu_1 \sin\theta}}\right)\right] \\
\sigma_{yy}^{(f)} &= \frac{K_I}{\sqrt{2\pi r}} \operatorname{Re}\left[\frac{1}{(\mu_1 - \mu_2)}\left(\frac{\mu_1}{\sqrt{\cos\theta + \mu_2 \sin\theta}} - \frac{\mu_2}{\sqrt{\cos\theta + \mu_1 \sin\theta}}\right)\right] \\
\sigma_{xy}^{(f)} &= \frac{K_I}{\sqrt{2\pi r}} \operatorname{Re}\left[\frac{\mu_1 \mu_2}{(\mu_1 - \mu_2)}\left(\frac{1}{\sqrt{\cos\theta + \mu_1 \sin\theta}} - \frac{1}{\sqrt{\cos\theta + \mu_2 \sin\theta}}\right)\right].
\end{aligned} \tag{36}$$

The homogenized displacements of the system can be written as:

$$\begin{aligned}
u^0 &= K_I \sqrt{\frac{2r}{\pi}} \operatorname{Re}\left[\frac{1}{(\mu_1 - \mu_2)}(p_2 \mu_1 \sqrt{\cos\theta + \mu_2 \sin\theta} - p_1 \mu_2 \sqrt{\cos\theta + \mu_1 \sin\theta})\right] \\
v^0 &= K_I \sqrt{\frac{2r}{\pi}} \operatorname{Re}\left[\frac{1}{(\mu_1 - \mu_2)}(q_2 \mu_1 \sqrt{\cos\theta + \mu_2 \sin\theta} - q_1 \mu_2 \sqrt{\cos\theta + \mu_1 \sin\theta})\right].
\end{aligned} \tag{37}$$

The respective Mode-II elastic fracture fields dominating the near-tip region of the layered systems under consideration take the form:

Mode-II micro stresses:

$$\begin{aligned}
\sigma_{xx}^{(m)} &= \frac{K_{II}}{\sqrt{2\pi r}} \operatorname{Re}\left[\frac{1}{(\mu_1 - \mu_2)}\left(\frac{\mu_2^{*(m)}}{\sqrt{\cos\theta + \mu_2 \sin\theta}} - \frac{\mu_1^{*(m)}}{\sqrt{\cos\theta + \mu_1 \sin\theta}}\right)\right] \\
\sigma_{yy}^{(m)} &= \frac{K_{II}}{\sqrt{2\pi r}} \operatorname{Re}\left[\frac{1}{(\mu_1 - \mu_2)}\left(\frac{1}{\sqrt{\cos\theta + \mu_2 \sin\theta}} - \frac{1}{\sqrt{\cos\theta + \mu_1 \sin\theta}}\right)\right] \\
\sigma_{xy}^{(m)} &= \frac{K_{II}}{\sqrt{2\pi r}} \operatorname{Re}\left[\frac{1}{(\mu_1 - \mu_2)}\left(\frac{\mu_1}{\sqrt{\cos\theta + \mu_1 \sin\theta}} - \frac{\mu_2}{\sqrt{\cos\theta + \mu_2 \sin\theta}}\right)\right]
\end{aligned} \tag{38}$$

$$\sigma_{xx}^{(f)} = \frac{K_{II}}{\sqrt{2\pi r}} \mathrm{Re}\left[\frac{1}{(\mu_1-\mu_2)}\left(\frac{\mu_2^{*(f)}}{\sqrt{\cos\theta+\mu_2\sin\theta}} - \frac{\mu_1^{*(f)}}{\sqrt{\cos\theta+\mu_1\sin\theta}}\right)\right]$$

$$\sigma_{yy}^{(f)} = \frac{K_{II}}{\sqrt{2\pi r}} \mathrm{Re}\left[\frac{1}{(\mu_1-\mu_2)}\left(\frac{1}{\sqrt{\cos\theta+\mu_2\sin\theta}} - \frac{1}{\sqrt{\cos\theta+\mu_1\sin\theta}}\right)\right]$$

$$\sigma_{xy}^{(f)} = \frac{K_{II}}{\sqrt{2\pi r}} \mathrm{Re}\left[\frac{1}{(\mu_1-\mu_2)}\left(\frac{\mu_1}{\sqrt{\cos\theta+\mu_1\sin\theta}} - \frac{\mu_2}{\sqrt{\cos\theta+\mu_2\sin\theta}}\right)\right]. \quad (39)$$

The homogenized mode-II displacements of the system can be written as:

$$u^0 = K_{II}\sqrt{\frac{2r}{\pi}} \mathrm{Re}\left[\frac{1}{(\mu_1-\mu_2)}\left(p_2\sqrt{\cos\theta+\mu_2\sin\theta} - p_1\sqrt{\cos\theta+\mu_1\sin\theta}\right)\right]$$

$$v^0 = K_{II}\sqrt{\frac{2r}{\pi}} \mathrm{Re}\left[\frac{1}{(\mu_1-\mu_2)}\left(q_2\sqrt{\cos\theta+\mu_2\sin\theta} - q_1\sqrt{\cos\theta+\mu_1\sin\theta}\right)\right]. \quad (40)$$

In the above micro mechanical fields given by eqns (35)–(40), we find that, except for σ_{xx}, the expressions for all other stress and displacement components are exactly the same as those given by Sih *et al.* (1965).

3. THE FINITE ELEMENT MODEL

The finite element solution of the full problem with detail micro structural heterogeneity is computationally extremely intensive. To circumvent this problem, a small near-tip region surrounding the physical crack-tip (See Figs 1 and 2) is considered for the finite element modeling. The dimensions of the near-tip region are so chosen that the region under consideration can be assumed to be fully confined inside the homogeneous orthotropic K-dominated asymptotic field such that the homogeneous orthotropic asymptotic displacements can be applied at the boundaries without introducing any appreciable error. This clearly requires that the dimension R of the *cut-out* region is sufficiently larger than the micro characteristic length l while being sufficiently smaller than a macro characteristic length such as the uncracked ligament size, the crack length or the specimen height. The near-tip boundary value problem is schematically shown in Fig. 2.

The near-tip solution domain comprises alternating layers of the *matrix* and the *fiber* consistent with the lamination morphology used in the development of the analytical model. The finite element representation of the domain is employed based on the eight-noded quadrilateral isoparametric elements. A typical finite element mesh used in this study is shown in Fig. 4 which is a representative of the mesh used for mixed-mode loading conditions. As seen in Fig. 4, a highly refined focused mesh is used in the immediate vicinity of the crack-tip which is surrounded by a rosette of singular quarter point elements in order to capture the expected square root singular stresses. Due to the symmetry associated with the mode-I loading, only the symmetric half of the mesh is considered for the mode-I analysis. In addition, for this loading case, symmetry boundary conditions consistent with mode-I loading, namely zero displacement in the y-direction and zero force in the x-direction, are imposed at all nodes in the crack-plane ahead of the crack-tip. While the crack surfaces are considered to be traction free for both the mode-I and mode-II loading cases, the homogeneous orthotropic asymptotic displacements are imposed on the remaining part of the boundary. The applied mixed-mode displacement field, which is characterized by the remote orthotropic stress intensity factor $K^0 = K_I^0 + iK_{II}^0$ with the mode-mixity $\Psi = \arctan(K_{II}^0/K_I^0)$ and modulus $|K^0|$ has the following form:

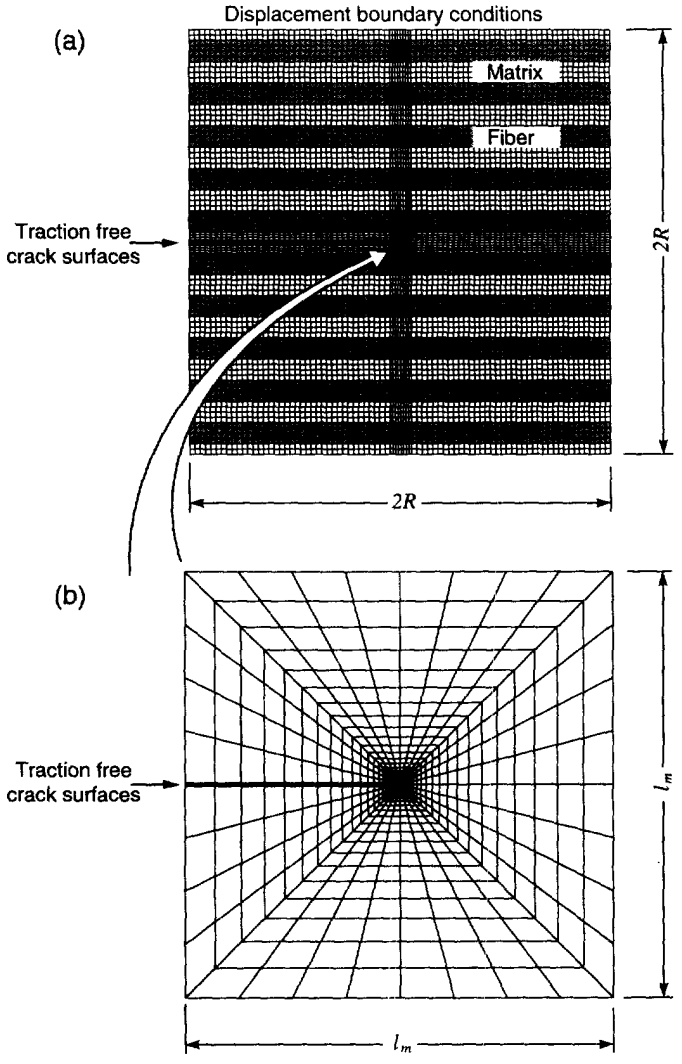

Fig. 4. (a) A typical finite element mesh using in solving the near-tip boundary value problem. (b) The focused near-tip mesh.

$$\begin{Bmatrix} u \\ v \end{Bmatrix} = |K^0| \sqrt{\frac{r}{2\pi}} \operatorname{Re} \begin{Bmatrix} U_{\mathrm{I}}(\theta, b_{ij}) \cos \Psi + U_{\mathrm{II}}(\theta, b_{ij}) \sin \Psi \\ V_{\mathrm{I}}(\theta, b_{ij}) \cos \Psi + V_{\mathrm{II}}(\theta, b_{ij}) \sin \Psi \end{Bmatrix} \tag{41}$$

where r and θ are the polar coordinates as shown in Fig. 2, b_{ij} are the compliances of the homogeneous orthotropic medium, and U_{I}, U_{II}, V_{I} and V_{II} are the spatial complex eigenfunctions obtained by solving the near-tip asymptotic problem for a homogeneous orthotropic medium. The subscripts I and II are used to denote mode-I and mode-II loading conditions, respectively. The explicit forms of these functions can also be found in Sih *et al.* (1965). The near-tip finite element solutions were obtained under plane strain conditions using the in-house finite element software DENDRO and were verified using general purpose finite element software ABAQUS.

4. RESULTS AND DISCUSSIONS

The results presented in this section are obtained for a bimaterial periodically layered system comprised of the isotropic matrix and the isotropic fiber layers with the fiber volume fraction $v_f = 0.5$. The ratio of the fiber modulus to that of the matrix is taken as $E_f/E_m = 10$ while the Poisson's ratio for both phases is taken to be $\nu_m = \nu_f = 0.3$. All computations

were performed in a non-dimensional environment to maintain the generality of the results. The spatial distances are normalized with the reference length R, the stresses are normalized with the reference stress $\sigma_0 = |K^0|/\sqrt{2\pi R}$ while the displacements are normalized with $U_0 = |K^0|/E_0\sqrt{R/2\pi}$. Here, $K^0 = K_I^0 + iK_{II}^0$ represents the homogeneous orthotropic complex stress intensity factor and E_0 is a reference elastic modulus which for this study is taken to be the matrix modulus E_m.

4.1. *Crack-plane stresses*

The mode-I normal stress σ_{yy} and the mode-II shear stress σ_{xy} acting on the crack-plane ahead of the crack-tip as predicted by finite elements analyses and the homogeneous orthotropic model are presented in Figs 5 and 6, respectively. The results for two layered systems, i.e., $E_f/E_m = 10$ and $E_f/E_m = 0.1$, are reported in these figures. Since the reference modulus, E_m, corresponds to the layer containing the delamination crack, the moduli ratio

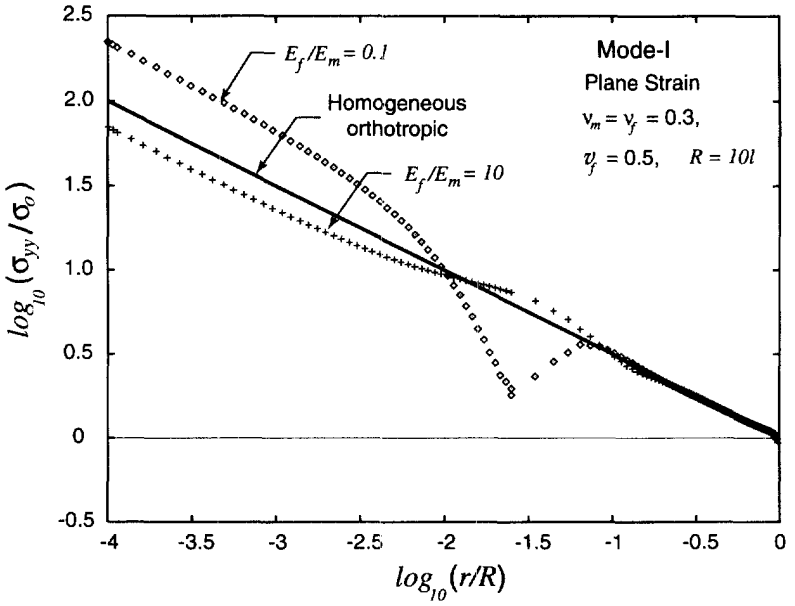

Fig. 5. Mode-I normal stress on the crack-plane ahead of the crack-tip.

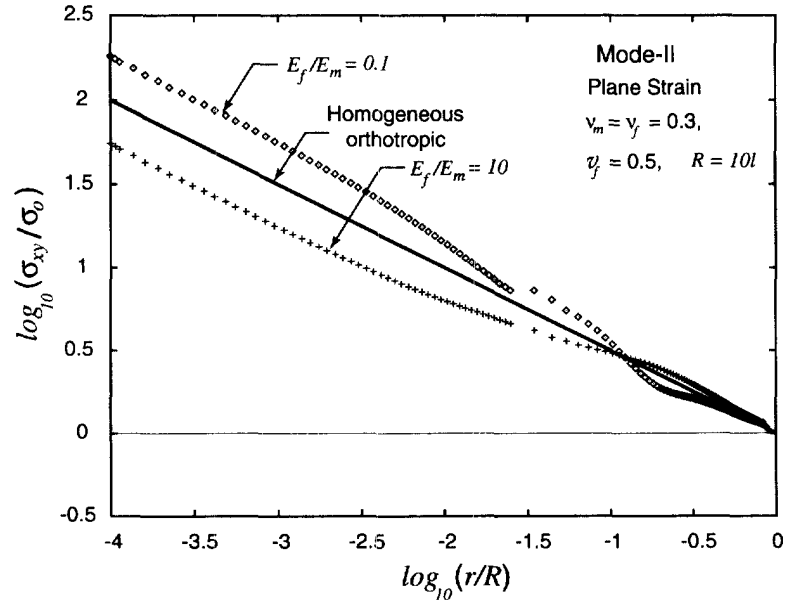

Fig. 6. Mode-II shear stress on the crack-plane ahead of the crack-tip.

$E_f/E_m = 10$ is associated with a system containing the delamination crack within a relatively compliant layer whereas the opposite applies for the $E_f/E_m = 0.1$ layered system. As discussed earlier in this study, the stress components σ_{yy} and σ_{xy} predicted by the analytical model in the systems under consideration are exactly the same as those predicted by the near-tip homogeneous orthotropic model. As such, the heavy solid lines in Figs 5 and 6 represent both the orthotropic predictions as well as the associated analytical solution. The results are plotted on a log-log scale such that the slope of the stress profile indicates the strength of the dominant singularity. It is to be noted that the stress field in the matrix material occupying the immediate vicinity of the crack-tip ($r/R < 0.01$) exhibits $r^{-1/2}$ behavior for both the pure mode-I and mode-II loadings. For a compliant matrix material, the stresses in the immediate vicinity of the crack-tip are found to be smaller than the homogeneous orthotropic prediction. As will be shown later on in this paper, the spatial distribution of the stress field in this region is independent of the global anisotropy of the system. However, the anisotropy of the system is shown to affect the stress distribution away from the crack-tip which asymptotes to the homogeneous orthotropic predictions in the far-field region. As shown in both Figs 5 and 6, all micro stress profiles obtained via finite elements exhibit a transitional regime which matches the isotropic near-tip predictions to the orthotropic far-field results. As shown, the extent of the transition region is limited within $0.01 \leqslant r/R \leqslant 0.1$ which is approximately equal to the thickness of a unit-cell.

4.2. *Stress intensity factors and energy release rates*

As discussed above, the singular stress field in a very small region surrounding the crack-tip is dominated by a local stress intensity factor, K^{tip}. While the structure of the asymptotic field in this region is governed by the matrix material, the dominating stress intensities are affected by the bimaterial properties. In order to establish the effects of the micro structure on the K^{tip}, we shall evaluate next the near-tip stress intensity, K^{tip}, using J-integral considerations. For the linear elastic layered systems under consideration which contain a crack parallel to the interfaces, the J-integral is path independent. As the J-integral physically represents the *crack driving force* or the energy release rate, $\mathcal{G}$, for linear elastic systems, the net expenditure of mechanical energy in the homogenized orthotropic domain is made available with no changes to the crack-tip such that:

$$\mathcal{G}^{\text{tip}} = \mathcal{G}^{\text{ortho}}. \tag{42}$$

The above equation can now be used to relate the near-tip $K_{\text{I}}^{\text{tip}}$ and $K_{\text{II}}^{\text{tip}}$ stress intensity components to their remotely applied orthotropic counterparts K_{I}^0 and K_{II}^0. More specifically, the orthotropic elastic energy release rate is given in terms of the material properties and the associated orthotropic stress intensity factor as follows:

$$\mathcal{G}_{\text{I}}^0 = (K_{\text{I}}^0)^2 \sqrt{\frac{b_{11}b_{22}}{2}}\left[\sqrt{\frac{b_{22}}{b_{11}}} + \frac{2b_{12}+b_{66}}{2b_{11}}\right]^{0.5} \text{ for mode-I} \tag{43}$$

and

$$\mathcal{G}_{\text{II}}^0 = (K_{\text{II}}^0)^2 \frac{b_{11}}{\sqrt{2}}\left[\sqrt{\frac{b_{22}}{b_{11}}} + \frac{2b_{12}+b_{66}}{2b_{11}}\right]^{0.5} \text{ for mode-II.} \tag{44}$$

At the same time, the stress intensity factor and energy release rate relation derived by Irwin for isotropic crack systems also applies in the matrix region around the crack-tip such that:

$$\mathcal{G}_{\mathrm{I}}^{\mathrm{tip}} = \frac{1-\nu_m^2}{E_m}(K_{\mathrm{I}}^{\mathrm{tip}})^2 \quad \text{for mode-I} \tag{45}$$

and

$$\mathcal{G}_{\mathrm{II}}^{\mathrm{tip}} = \frac{1-\nu_m^2}{E_m}(K_{\mathrm{II}}^{\mathrm{tip}})^2 \quad \text{for mode-II.} \tag{46}$$

When combining eqns (43) and (45) the mode-I tip intensity factor is found to be:

$$K_{\mathrm{I}}^{\mathrm{tip}} = K_{\mathrm{I}}^{0}\left[\frac{E_m}{1-\nu_m^2}\sqrt{\frac{b_{11}b_{22}}{2}}\left\{\sqrt{\frac{b_{22}}{b_{11}}}+\frac{2b_{12}+b_{66}}{2b_{11}}\right\}^{0.5}\right]^{0.5} \tag{47}$$

whereas by combing eqns (44) and (46) the mode-II tip component is found to be:

$$K_{\mathrm{II}}^{\mathrm{tip}} = K_{\mathrm{II}}^{0}\left[\frac{E_m}{1-\nu_m^2}\frac{b_{11}}{\sqrt{2}}\left\{\sqrt{\frac{b_{22}}{b_{11}}}+\frac{2b_{12}+b_{66}}{2b_{11}}\right\}^{0.5}\right]^{0.5}. \tag{48}$$

When both $K_{\mathrm{I}}^{\mathrm{tip}}$ and $K_{\mathrm{II}}^{\mathrm{tip}}$ are acting simultaneously, the mixed-mode field at the crack-tip is dominated by the tip stress intensity factor $K^{\mathrm{tip}} = K_{\mathrm{I}}^{\mathrm{tip}} + iK_{\mathrm{II}}^{\mathrm{tip}}$. Clearly, through eqns (47) and (48) it is noticed that the relative amounts of mode-I and mode-II dominating the crack-tip region may be different from their applied counterparts. This results in a phase shift between the remotely applied and the induced tip mixed-mode loading. The tip mode-mixity, i.e. $\Psi^{\mathrm{tip}} = \arctan(K_{\mathrm{II}}^{\mathrm{tip}}/K_{\mathrm{I}}^{\mathrm{tip}})$, can be obtained with the aid of eqns (47) and (48) as follows:

$$\tan\Psi^{\mathrm{tip}} = \left(\frac{b_{11}}{b_{22}}\right)^{0.25}\tan\Psi \tag{49}$$

where, as before, $\Psi = \arctan(K_{\mathrm{II}}^{0}/K_{\mathrm{I}}^{0})$ is the applied mode-mixity. It is important to note that the effective tip phase angle depends only on the homogenized properties and remains the same whether the crack lies in the compliant or in the stiffer material phase of a bimaterial layered system.

The mode-I tip stress intensity factor predicted by eqn (47) is plotted as solid lines against the bimaterial moduli ratio E_f/E_m for various fiber volume fractions in Fig. 7. The

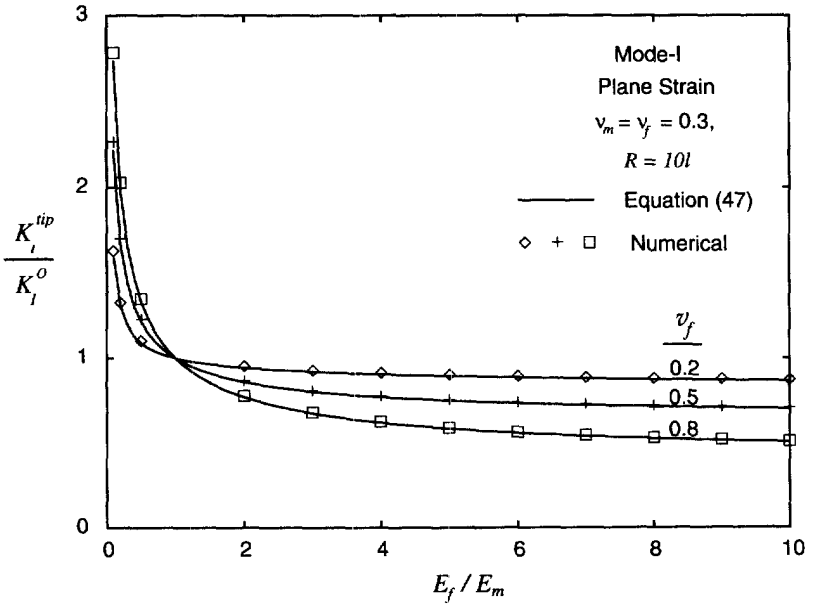

Fig. 7. Normalized tip stress intensity factor for mode-I loading.

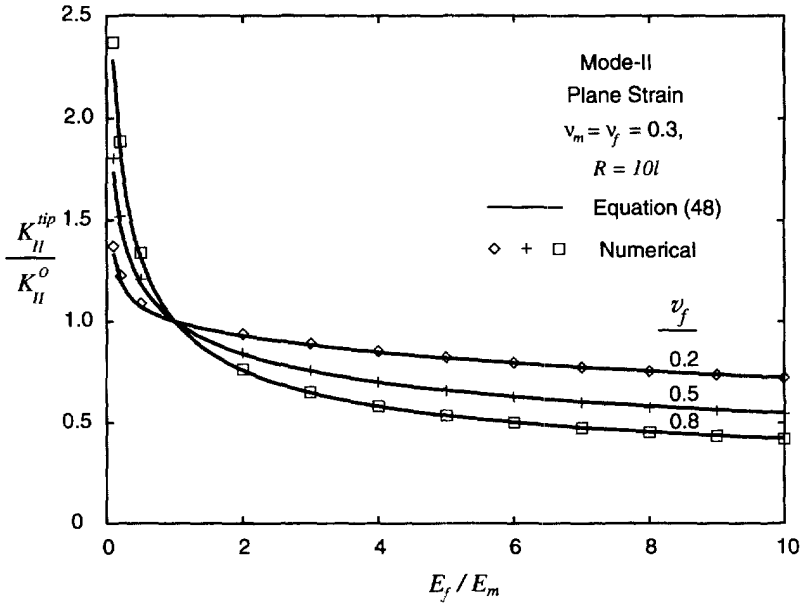

Fig. 8. Normalized tip stress intensity factor for mode-II loading.

discrete points in Fig. 7 represent the values obtained numerically using the stiffness derivative method (Parks, 1974). The numerical results are shown to be in excellent agreement with those predicted via eqn (47). It is also observed in Fig. 7 that by increasing the fiber volume fraction, v_f, higher shielding effects are produced for systems with $E_f/E_m > 1$. On the other hand, as v_f increases, stress intensity amplification is shown to take place in systems with $E_f/E_m < 1$. The effects of the bimaterial moduli ratio and the fiber volume fraction on the mode-II tip stress intensity factor, K_{II}^{tip}, are presented in Fig. 8. The predictions of eqn (48) are plotted as solid lines and the numerically obtained values are overlaid as discrete points. Both results are found to be in excellent agreement. The crack-tip amplification and shielding exhibited in pure mode-II loading are found to exhibit trends very similar to those exhibited under mode-I loading.

The phase shift $\Delta\Psi = \Psi^{tip} - \Psi$ obtained from eqn (49) for the mixed-mode loading is plotted against the applied phase angle Ψ in Fig. 9 for different values of the parameter

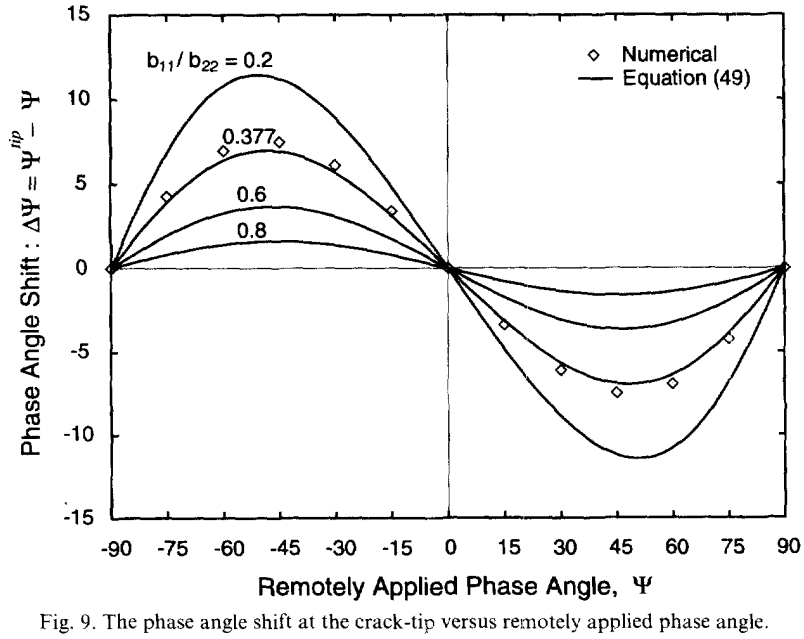

Fig. 9. The phase angle shift at the crack-tip versus remotely applied phase angle.

b_{11}/b_{22} which depends on the material combination and the fiber volume fraction. In order to verify eqn (49), a number of near-tip boundary value problems with different mode mixities were solved numerically and the phase shift was calculated using the energy based technique of Matos *et al.* (1989). The material system chosen for this purpose had $E_f/E_m = 10$ and $v_f = 0.5$ and $v_f = v_m = 0.3$ with the crack-tip located in the compliant phase. The numerically calculated phase shift for this bimaterial system which corresponds to $b_{11}/b_{22} = 0.377$ are overlaid in Fig. 9 as discrete points. The predictions of eqn (49) with $b_{11}/b_{22} = 0.377$ for the above system are observed to be in good agreement with the corresponding finite elements results. For the periodically layered bimaterial systems with isotropic layers, the ratio b_{11}/b_{22} is always less than one and therefore in accordance with the results shown in Fig. 9, the local phase angle Ψ^{tip} is predicted to be less than the applied phase angle Ψ.

4.3. *Mode-I micro stress angular profiles*

The angular variations of the normalized micro-stress components σ_{xx}, σ_{yy} and σ_{xy} at normalized radial distances $r/R = 0.001$ and 0.8 are presented in Fig. 10. Since the matrix phase surrounding the physical crack-tip is isotropic, the stress profiles at $r/R = 0.001$ are accompanied with the isotropic singular solution. The stress intensity factor for the isotropic field was obtained with the aid of eqn (47). It is seen from the left column in Fig. 10 that

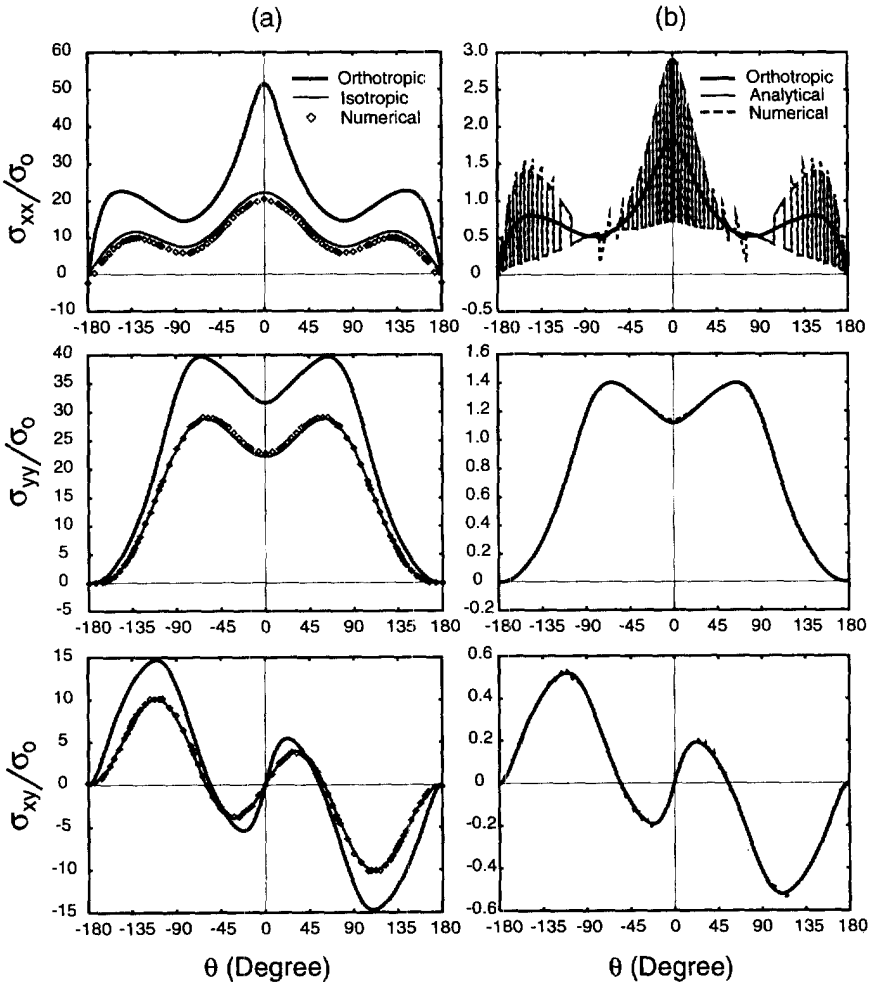

Fig. 10. Angular variation of micro stresses in plane strain mode-I loading. (a) In the matrix phase surrounding the crack-tip at $r = 0.001R$. (b) In the far-field region at $r = 0.8R$. The above results correspond to $E_f/E_m = 10$, $v_f = v_m = 0.3$, fiber volume fraction $v_f = 0.5$ and dual length ratio $R/l = 10$. The reference stress is taken as $\sigma_o = |K^0|/\sqrt{2\pi R}$.

the stresses in the immediate vicinity of the crack-tip are considerably lower compared to the anisotropic continuum predictions and are in excellent agreement with the isotropic field solutions which are dominated by the tip stress intensity factor K_I^{tip}.

The angular variation of stresses in the far field region at radial distances $r/R = 0.8$ is shown in the right column of Fig. 10. It is seen that the stress components σ_{yy} and σ_{xy} are continuous owing to the continuity requirements of the traction at the fiber/matrix interfaces and they are in excellent agreement with their anisotropic continuum counterparts. The heterogeneous micro structure induced discontinuity is reflected in σ_{xx} which oscillates about the anisotropic continuum prediction. This oscillation of σ_{xx} is captured by the eigenfunctions which are given in eqns (35) and (36). For all stress components, the predictions of the analytical model are found to be in a remarkable agreement with the numerical solutions obtained via the method of finite elements. The stresses in the far-field region are dominated by the remotely applied stress intensity factor.

4.4. *Mode-II micro stress angular profiles*

In Fig. 11, the angular variations of the normalized stress components are presented for the pure mode-II loading. As before, the results are reported for $r = 0.001R$ and $r = 0.8R$. The isotropic analytical predictions presented in the left column of Fig. 11 were obtained using the tip stress intensity factor, K_{II}^{tip}, which is given by eqn (48). It is observed

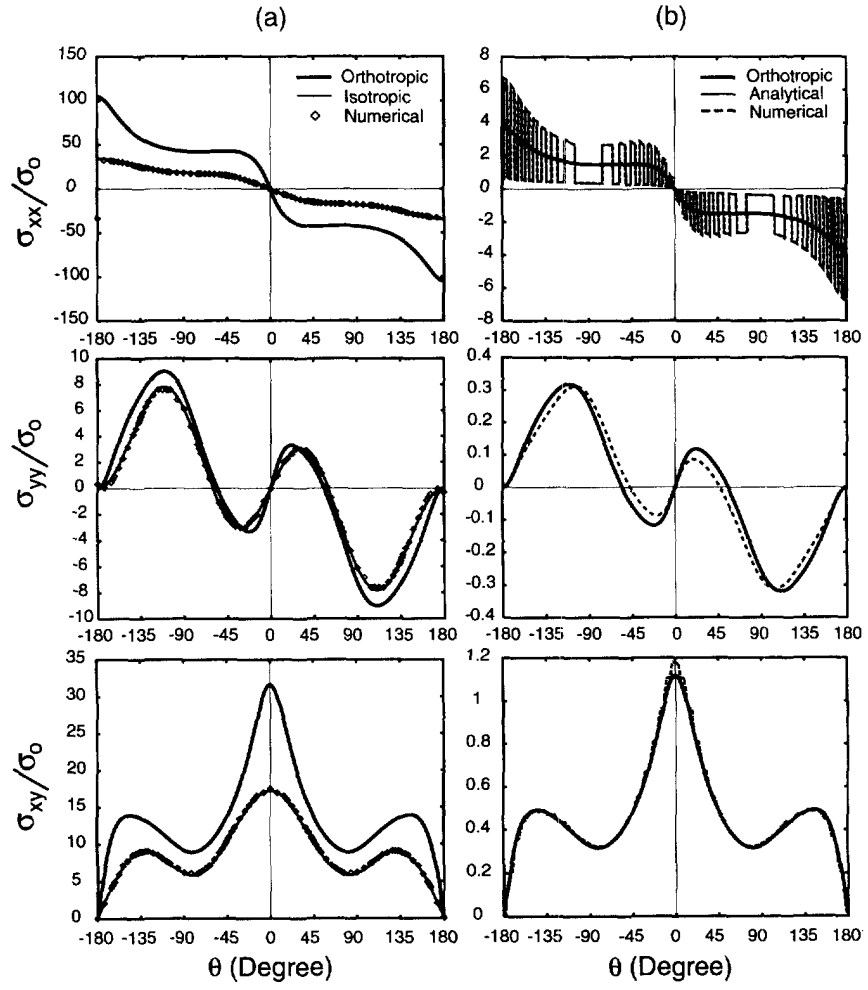

Fig. 11. Angular variation of micro stresses in plane strain mode-II loading. (a) In the matrix phase surrounding the crack-tip at $r = 0.001R$. (b) In the far-field region at $r = 0.8R$. The above results correspond to $E_f/E_m = 10$, $\nu_f = \nu_m = 0.3$, fiber volume fraction $v_f = 0.5$ and dual length ratio $R/l = 10$. The reference stress is taken as $\sigma_o = |K^0|/\sqrt{2\pi R}$.

that the numerically predicted stress field in the immediate vicinity of the crack-tip exhibits universal isotropic behavior. The far-field stresses under mode-II loading are shown in the right column of Fig. 11. The analytical and numerical predictions for both stress component σ_{xx} and σ_{xy} are found to overlap each other to such an extent that the analytical and numerical results can not be distinguished easily. As expected, the micro-stress σ_{xx} oscillates about the homogeneous orthotropic prediction. The agreement between the analytical and numerical predictions of σ_{xx} is found to be relatively better in the softer matrix layers compared to that in the stiffer fiber layers.

4.5. *Mixed-mode micro stress angular profiles*

The angular variation of the normalized micro stresses for the mixed-mode loading is shown in Fig. 12. The mode-mixity angle, $\Psi = \arctan(K_{II}^0/K_I^0)$, for the applied loading has been taken to be 45° which implies equal amount of applied mode-I and mode-II loading. As before, the variations of the micro stresses are presented for the immediate crack-tip neighborhood at a radial distance of $r/R = 0.001$ and for the far-field region at a radial distance of $r/R = 0.8$. The local tip stress intensity factors K_I^{tip} and K_{II}^{tip} dominating the matrix material surrounding the crack-tip were taken to be those predicted by eqns (47) and (48). The isotropic field shown in the left column of Fig. 12 represented by a continuous thin line is that dominated by the effective tip stress intensity factor $K^{tip} = K_I^{tip} + iK_{II}^{tip}$. It is interesting to note that the stresses in the immediate vicinity of the crack-tip do exhibit an isotropic field behavior but in accordance with eqn (49) the phase angle dominating the

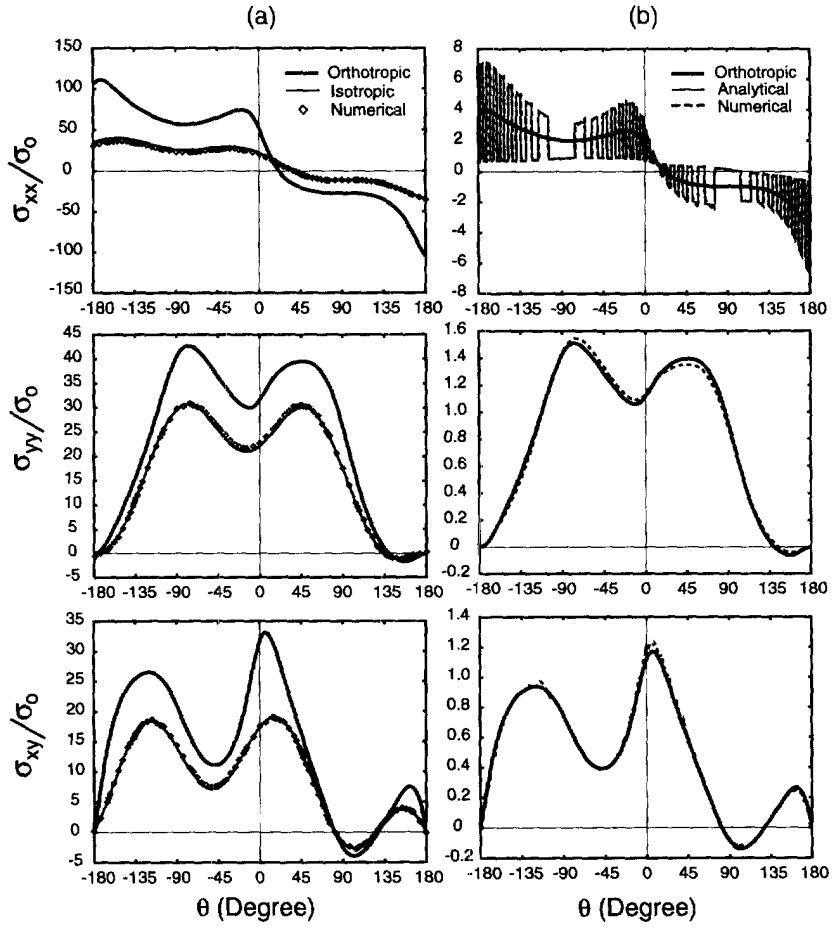

Fig. 12. Angular variation of micro stresses in plane strain mixed-mode loading with $\Psi = 45°$. (a) In the matrix phase surrounding the crack-tip at $r = 0.001R$. (b) In the far-field region at $r = 0.8R$. The above results correspond to $E_f/E_m = 10$, $\nu_f = \nu_m = 0.3$, fiber volume fraction $v_f = 0.5$ and dual length ratio $R/l = 10$. The reference stress is taken as $\sigma_o = |K^0|/\sqrt{2\pi R}$.

matrix region surrounding the crack-tip, $\Psi^{tip} = \arctan(K_{II}^{tip}/K_{II}^{tip})$, is different from the phase angle Ψ of the applied loading. This happens due to the effects of global anisotropy of the system which changes scaling factors for the two modes of the applied loading.

The angular variation of the stress in the far-field region at radial distances $r/R = 0.8$ under mixed-mode loading is shown in the right column of Fig. 12. It is seen that the discontinuous micro stress σ_{xx} oscillates about the mean stress represented by the thick solid line. For all stress components, the predictions of the analytical model are found to be in a remarkable agreement with the numerical solutions obtained via the method of finite elements. As expected, the stresses in the far-field region are found to be dominated by the remotely applied stress intensities.

4.6. *Contour plots*

The mode-I contour plots in the region close to the crack-tip which were obtained numerically via the method of finite elements as well as those obtained analytically are shown in Fig. 13. The contour levels are indicated in the figure by means of a side color bar attached with each plot. For comparison purposes, the numerical stress contour plots are reported on the left under column (a) whereas their analytical counterparts are reported on the right under column (b). Similar contour levels were selected for both the numerical and analytical results. We clearly notice that the stress component σ_{xx} is discontinuous while σ_{yy} and σ_{xy} are continuous throughout the region. The analytically predicted contour plots are found to be smooth compared to those predicted numerically. The non-smoothness of the numerically predicted contours is believed to be partly due to the nonlocal effects which are not accounted by the approximate analytical model and partly due to the mesh discretization used in the analysis. As mentioned earlier, the current analytical model can be extended to predict more realistic stress field by including some higher order terms. Nevertheless, all important features of the stress field are nicely captured by the current analytical model.

The contours of the micro stresses obtained numerically and analytically in the near-tip detailed region for pure mode-II loading are shown in Fig. 14. The contour levels are adjusted to values that best reveal the important features of the stress field. As expected, σ_{yy} and σ_{xy} are found to be continuous throughout the region while σ_{xx} is shown to be discontinuous at all matrix/fiber interfaces. For pure mode-II loading, the analytical predictions are found to be very close to the numerical predictions. The stress components σ_{xy} is observed to attain a maximum value while as expected, σ_{xx} and σ_{yy} vanish on the crack plane ahead of the crack-tip. The normal stresses are shown to dominate the area below the crack-tip consistent with the mode-II fields in homogeneous systems.

Figure 15 shows the contours of the normalized micro stresses on the deformed geometry for mixed-mode loading in a detailed region surrounding the crack-tip. As shown in the above figure, the applied mode-mixity phase angle for these contours is 45°. An excellent agreement between the numerical and analytical contours is observed. As expected, the stress components σ_{yy} and σ_{xy} are continuous throughout the near-tip heterogeneous region. The light grey region surrounding the crack-tip in the σ_{xx} contour plots is rather revealing on the shape of potential crack renucleation zone in layered systems.

4.7. *Interfacial stresses*

The normal and shear stresses acting on the interfaces closest to the crack plane directly above and below the crack tip are shown in Fig. 16. The mode-I predictions are reflected in the top row of plots, the mode-II results are shown in the middle row whereas the mixed mode results are those in the bottom row of plots of Fig. 16. As before, the stresses are normalized with the reference stress σ_o. The data points shown in Fig. 16 represent the finite element predictions whereas the solid lines represent the predictions of the approximate analytical model. These results were obtained for the same bimaterial layered system used to obtain the results earlier in this work. As such, the interfacial finite element stresses reported in Fig. 16 represent transient regime results and are thus, not expected to be in agreement with the analytical model prediction. As shown in Fig. 16 however, the analytical and finite element results are found to be in a remarkably good agreement for the mode-I

loading case whereas the results are in lesser agreement for the mode-II and therefore the mixed-mode loading cases. The mixed-mode results shown in the third column of plots include the interface stresses acting at both the top and the bottom interfaces. The model-I and II stresses were plotted only for the upper interface since the stresses acting on the lower one can be extracted from the reported results using symmetry arguments.

In addition to enabling further comparison between the analytical and numerical predictions, the results reported in Fig. 16 may also offer useful insights on the potential for crack renucleation and interface delamination under ideally brittle conditions for the systems and loading considered herein. It is clearly shown in Fig. 16 that the interfacial stresses of relatively high magnitude compared to the reference stress may dominate the interface region directly above and below the crack-tip. This high interface stress zone is shown to be limited within the interval $-0.1 \leqslant x/l_m \leqslant 2$ which represents approximately the length of one fiber/matrix unit-cell.

5. CRACK LOCATION EFFECTS

As discussed earlier, the approximate analytical model presented in this work yields a rather accurate description of the stress fields in an area bounded on the outside by the boundary of the near-tip *cut-out* region used in this study and in the inside by a radial distance from the crack tip which was shown to be of the order of one to two unit-cell lengths. In separate studies (see Jha *et al.*, 1997), it is shown that the elastic singular fields dominating the above annular area remain rather unaffected by the location of the crack relative to its adjacent parallel interfaces. On the contrary, in those studies it is shown that the fields dominating the near-tip region surrounding the physical crack tip remain sensitive to the location of the crack within the layer and its relative distance from the adjacent interfaces.

In order to demonstrate some of the above findings, in this section, we conduct numerical finite element studies as needed to assess the effects on the near-tip mechanics of the location of the major crack relative to its adjacent interfaces. The boundary value problem for this study is set up using the same heterogeneous *cut-out* near-tip area shown in Fig. 2. However, in deriving the results for this part of the study, instead of considering the crack to be located in the middle of the layer, the crack was placed at several discrete distances t/l_m from its adjacent bottom interface. As such, the homogeneous orthotropic displacement fields imposed along the boundary of the *cut-out* domain were evaluated with respect to the off-set location of the crack-tip. The values for t/l_m considered for this part of the study were in the interval $0.1 \leqslant t/l_m \leqslant 0.9$.

The exact crack location for each of the nine cases considered can be extracted from the finite element data points shown in every plot in Fig. 17. Values for t/l_m outside the above interval were not considered, since other bimaterial effects due to layer proximity become more important and thus may influence the near-tip mechanics for cracks located adjacent to either the top or the bottom interface. For example, when $t/l_m = 0$ the near tip solution should be that obtained for an interface crack bounded by the matrix material on the top and the fiber material at the bottom. On the other hand, when $t/l_m = 1.0$, then the near tip solution should be that obtained for an interface crack bounded by the matrix material on the bottom and the fiber material at the top. The latter solutions are presented and compared to the finite element results obtained using the approach described in this section in the paper by Jha *et al.* (1997). Thus, in this section, we limit our interest to those solutions that exhibit in a clear way the isotropic characteristics for the matrix near-tip asymptotic elastic fields. For the sake of clarity of the results, a new tip stress intensity factor, $\bar{K}^{\text{tip}} = \bar{K}_{\text{I}}^{\text{tip}} + i\bar{K}_{\text{II}}^{\text{tip}} = |\bar{K}^{\text{tip}}| \cdot \bar{\Psi}^{\text{tip}}$ will be used in association with the isotropic matrix tip fields dominating the near-tip region of the offset crack-tip.

The normalized $\bar{K}_{\text{I}}^{\text{tip}}$ and $\bar{K}_{\text{II}}^{\text{tip}}$ components of the local offset tip stress intensity factor as a function of the normalized distance t/l_m from the bottom interface are presented in Fig. 17. The above figure includes the results for three loading cases. More specifically, the plots in the top row correspond to a remotely applied pure mode-I loading. The plots in the middle row of Fig. 17 were obtained for an applied pure mode II loading whereas those

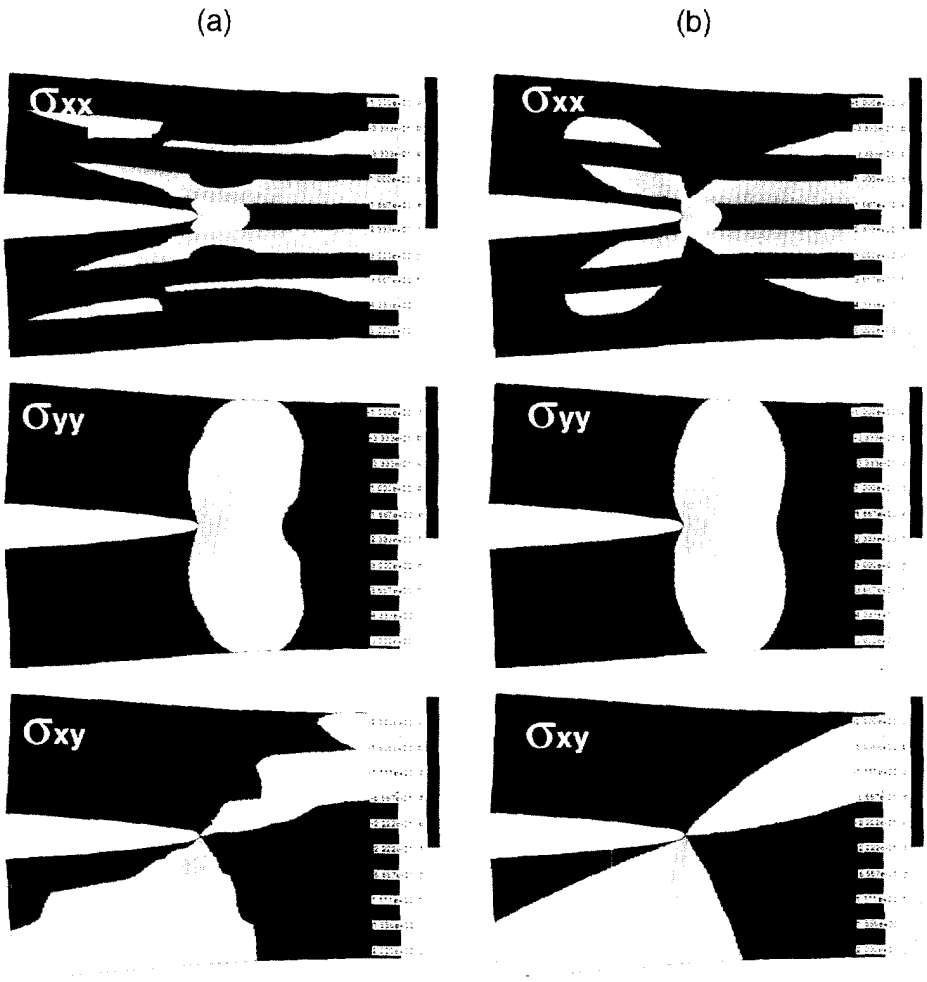

Fig. 13. Stress contours in a detailed region around the crack-tip under mode-I loading. Column (a): Finite elements predictions. Column (b): Approximate analytical model.

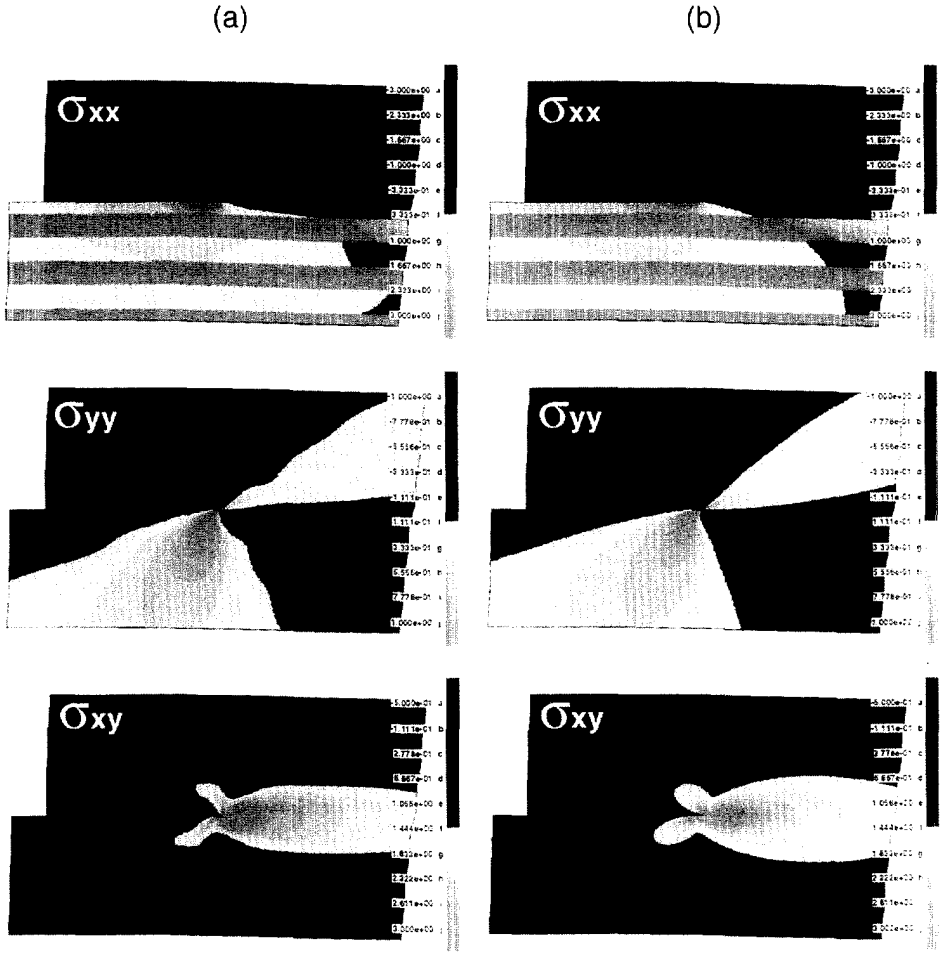

Fig. 14. Stress contours in a detailed region around the crack-tip under mode-II loading. Column (a): Finite elements predictions. Column (b): Approximate analytical model.

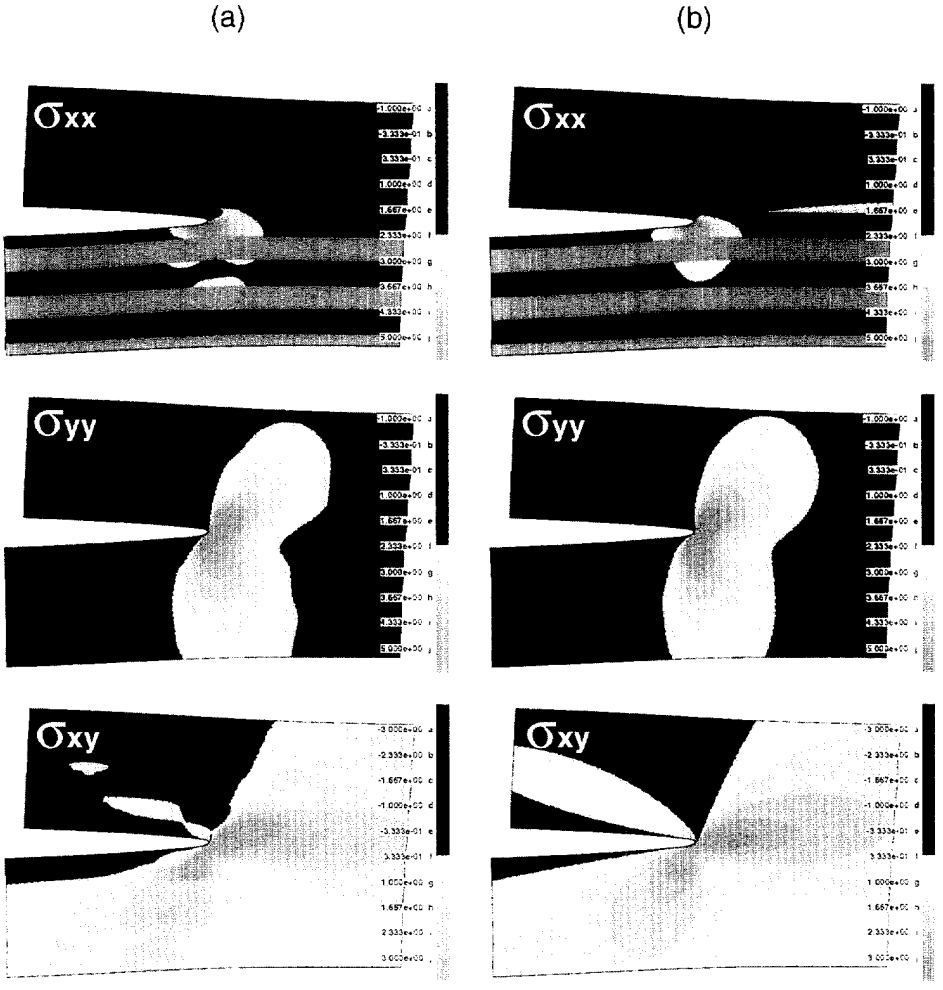

Fig. 15. Stress contours in a detailed region around the crack-tip under mixed-mode loading with remotely applied phase angle $\Psi = 45^{\circ}$. Column (a): Finite elements predictions. Column (b): Approximate analytical model.

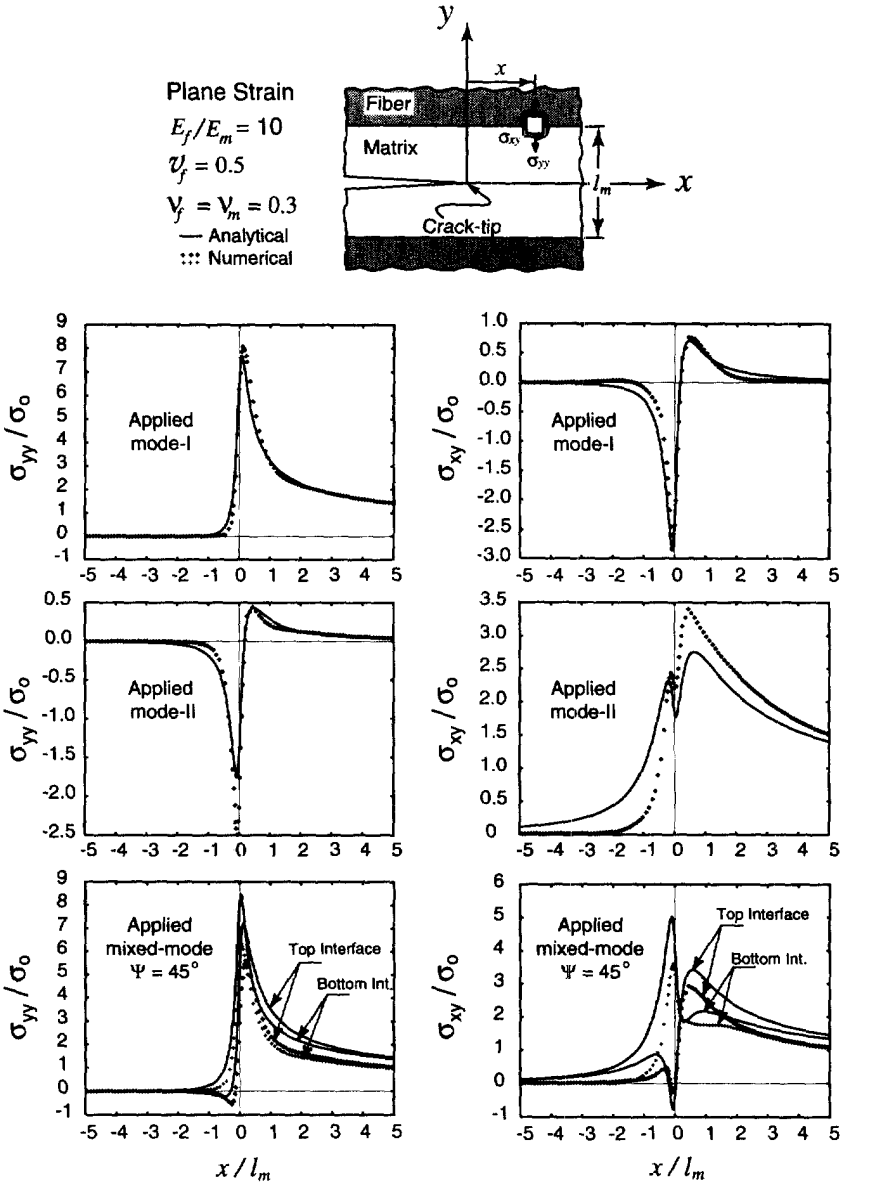

Fig. 16. Stresses along the first interface directly above the crack plane. The reference stress is taken as $\sigma_o = |K^0|/\sqrt{2\pi R}$.

in the third row were obtained for an applied mixed mode loading corresponding to equal amounts of mode-I and II loading, i.e., $\Psi = 45$ degrees. For each loading case, the plots in the left column represent the normalized mode-I component of the offset crack-tip stress intensity factor $\bar{K}_I^{tip}$, whereas the right column represents the associated mode-II component for the loading cases considered.

Thus, the normalized $\bar{K}_I^{tip}$ and $\bar{K}_{II}^{tip}$ components of the local offset crack-tip stress intensity factor obtained under an applied pure mode-I loading plotted against the normalized distance t/l_m from the bottom interface are shown in the top row of plots in Fig. 17. As before, these local tip mixed mode results were extracted from the associated finite element solutions using the energy method developed by Matos *et al.* (1989). Based on these results, two major observations can be made.

The first observation is that under an apparent/applied mode I loading, a very small matrix region around the offset crack-tip which is within the layer containing the crack may be dominated by slightly mixed-mode conditions. Local pure mode-I conditions are shown to be obtained only for systems wherein the crack is placed in the middle of the

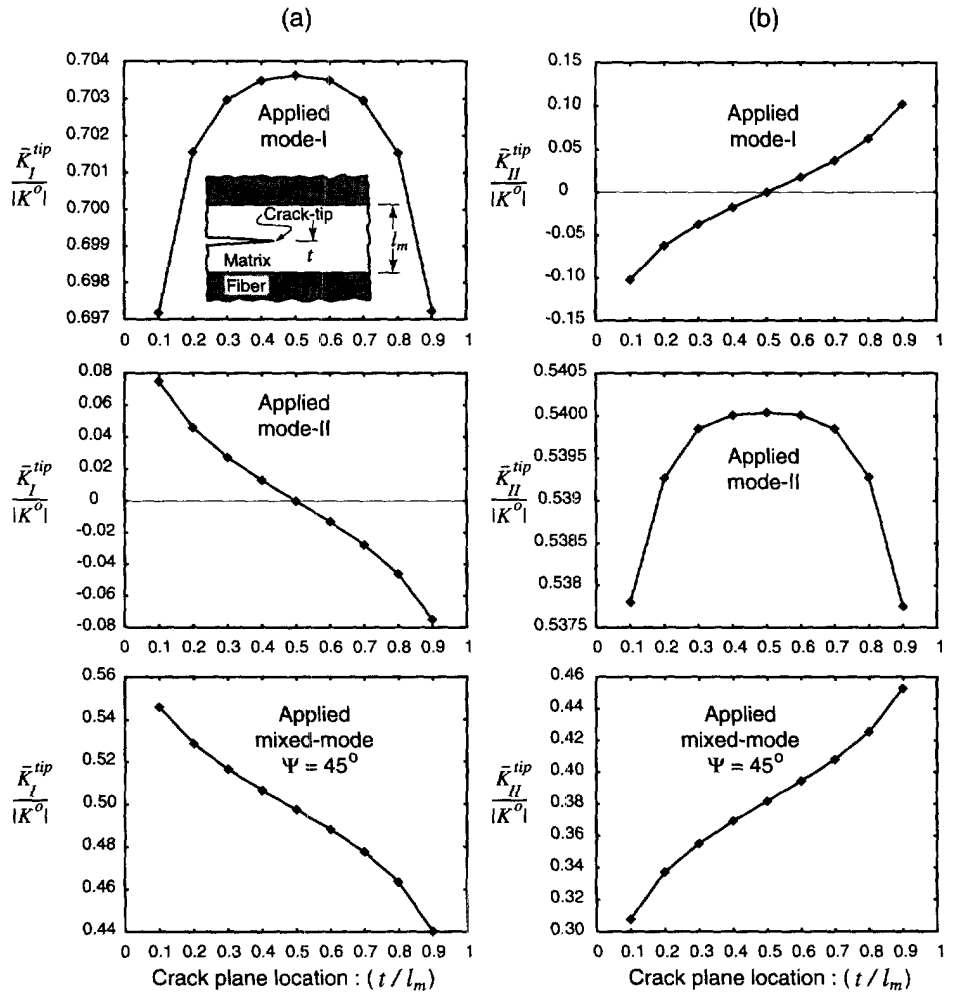

Fig. 17. Variation of the tip stress intensity factors with the crack location relative to the adjacent interfaces. The results in the top row of plots correspond to an applied mode-I loading, those in the middle row to pure mode-II and the bottom row results were obtained for an applied mixed-mode loading.

matrix layer as assumed by the approximate analytical model. For cracks however located at distances closer to either of the two adjacent interfaces, the results presented in the top row in Fig. 17 suggest that the opening or mode-I tip component of the stress intensity factor reduces slightly while a non-zero mode-II component develops. The presence of a non-zero mode II predicted for cracks located away from the middle of the matrix layer, is also shown in Fig. 18b in terms of a non-zero mode mixity. This figure suggest that over the range of normalized distances from the bottom interface considered, a maximum phase angle shift of about 8 degrees is predicted for the two extreme cases considered. over the same range, it is also shown in Fig. 18a that the associated elastic energy release rate remains constant and as such it does not depend on the relative location of the crack within the layer.

The second major observation that can be made using the results shown in Figs 17 and 18, is that the near-tip region dominated by $\bar{K}^{tip}$ experiences the same mode mixity as the applied one only for cracks located in the middle of the layer and subjected to either pure mode-I or pure mode-II loading. For example, in the latter cases, local pure mode-I conditions are obtained when an overall pure mode-I loading is applied whereas local pure mode-II conditions are predicted when a remote pure mode-II loading is applied. It is interesting however to notice that under the above conditions, the micro structure appears to effectively reduce the dominant local stress intensities. For example, for cracks placed in

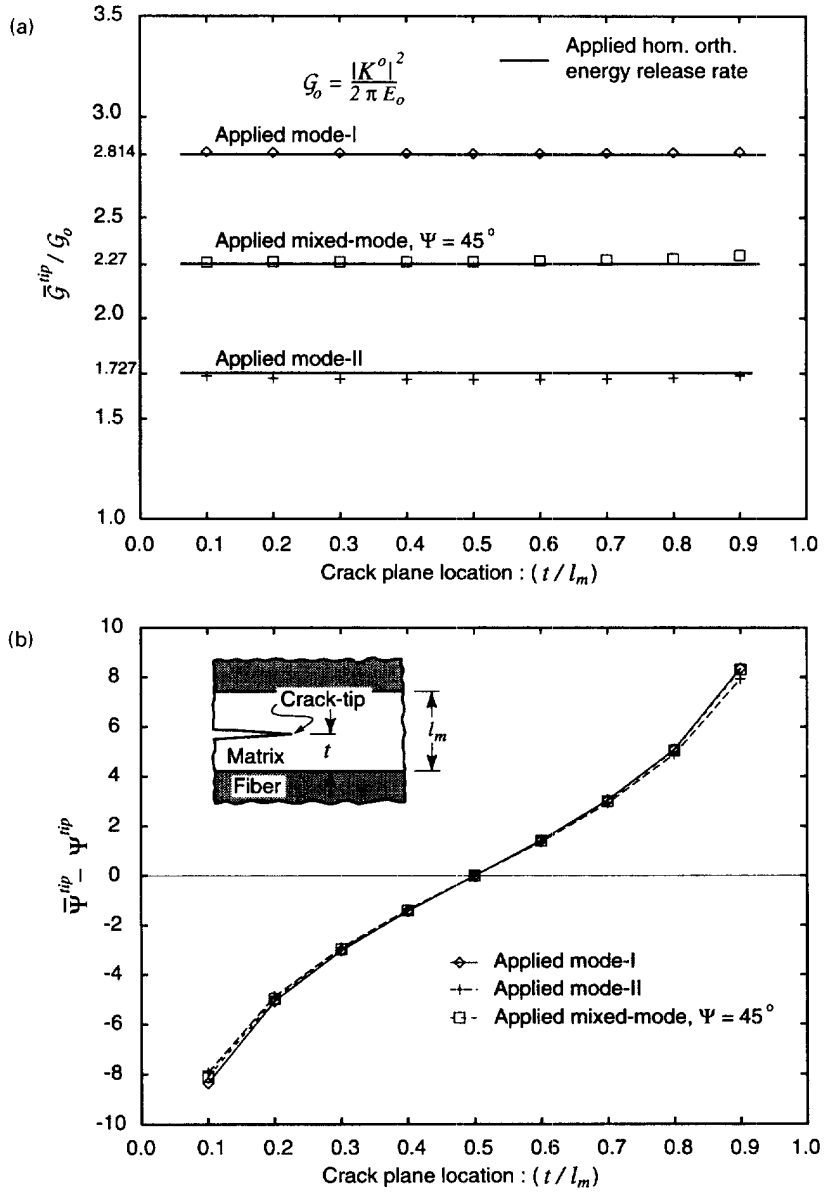

Fig. 18. (a) The normalized elastic energy release rate in the matrix phase surrounding the offset crack-tip under remotely applied mode-I, mode-II and mixed-mode loading. (b) The phase shift of the offset crack with respect to the phase angle of the mid-plane crack.

the middle of the layer and under pure mode I applied loading the effective tip stress intensity factor is predicted to be $\bar{K}_I^{tip} = K_I^{tip} = 0.7K_I^0$ and under pure mode-II applied loading of the corresponding mode-II component of the local stress intensity factor is predicted to be only $\bar{K}_{II}^{tip} = K_{II}^{tip} = 0.54K_{II}^0$. This type of effective shielding of the local tip fields from the applied loads is clearly influenced by the layer micro structure and bimaterial properties as discussed earlier in this work.

The local tip stress intensities associated with a remote pure mode-II loading are shown in the second row of plots in Fig. 17. Under these conditions, $\bar{K}_{II}^{tip}$ appears to behave in a similar manner as the $\bar{K}_I^{tip}$ did under the influence of pure mode-I applied loading which was discussed above. This type of reciprocal behavior appears to also apply for the $\bar{K}_I^{tip}$ induced by a remote pure mode-II loading and the negative of $\bar{K}_{II}^{tip}$ induced by a remote pure mode-I loading.

In Fig. 18a, the energy release rate made available to the local offset crack tip is plotted against the normalized distance t/l_m of the crack plane from the bottom interface. It is of

interest to observe that for all three loading cases considered, the $\bar{\mathcal{G}}^{tip}$ remains constant and independent of the crack location within the layer. This can be explained by considering the path independence of the J-integral along side with the argument of imposing for the cracked systems of *infinite dimensions* under consideration the same applied elastic energy release rate through the use of the same orthotropic near-tip displacement fields.

In Fig. 18b, the difference of the mode mixity dominating the local crack tip region i.e., $\bar{\Psi}^{tip}$, to the mode mixity dominating the same region of a crack placed in the middle of the layer i.e., Ψ^{tip}, is plotted against the normalized distance t/l_m. As expected, the above phase shift becomes zero for $t/l_m = 0.5$ and takes on a maximum value of about 8 degrees for the extreme cases considered of $t/l_m = 0.1$ and $t/l_m = 0.9$. It is worth noticing that similar predictions are obtained for all three loading cases considered. As mentioned earlier in this section, a more thorough presentation on the crack location effects for the systems considered in this study as well as for layered systems with cracks placed perpendicular to the interfaces is included in a forthcoming article.

6. CONCLUDING REMARKS

The mode-I, mode-II and mixed mode asymptotic near-tip fields associated with cracks placed parallel to the interfaces of a layered bimaterial system have been developed both analytically using asymptotic homogenization and numerically using the method of finite elements. Two distinct regions of K-dominance have been observed. The matrix region surrounding the crack-tip of the crack embedded in the middle of the layer was shown to be dominated by a local tip stress intensity factor $K^{tip} = K_I^{tip} + iK_{II}^{tip}$. At the same time, the stress fields dominating material points at radial distances greater than approximately one or two fiber/matrix unit-cell lengths were shown to be expressed in terms of the applied orthotropic stress intensity factor $K^0 = K_I^0 + iK_{II}^0$. In this annular domain, the continuous stress components were predicted with sufficient accuracy using the orthotropic spatial eigenfunctions. However, the discontinuous normal stress component which is parallel to the interfaces was shown to deviate substantially from its orthotropic counterpart and it was nicely captured by the analytical approximate model. The analytical results were shown to be in good agreement with those obtained via the method of finite elements. Observed micro-stress deviations were attributed to layer proximity and higher order strain gradient effects which are not accounted by the approximate analytical model.

The relations between the local K^{tip} and the remotely applied K^0 have been established. Consistent with the path independence of the J-integral, it has been shown that for the class of system considered in this study, the linear elastic energy release rate made available to the crack tip is equal to its applied orthotropic counterpart. At the same time, it was shown that an appreciable shift in the tip phase angle compared to the applied one was induced as a result of the layered micro structure. An additional phase shift was also observed in systems containing cracks away from the middle of the layer.

In light of the above findings, it is concluded that the analytical model developed herein provides an excellent tool for the description of the micro mechanical fields dominating the near-tip region of layered systems that belong in the general family of layered composites considered in this study. As such, the results presented herein can be used to predict the onset of delamination fractures in stratified composites and the evolution of other small scale non-linear phenomena such as plasticity in metal layers and microcracking that may develop in the brittle layers within the near-tip region during delamination fracture.

Acknowledgments—Support for this work was provided by the National Science Foundation through a Presidential Young Investigator award, grant CMS94-96209. The authors would like to express their gratitude to Professor R. Ballarini of Case Western Reserve University, Cleveland, Ohio, for helpful discussions on this work and to Jonathan L. Kuhn for his logistical support in making effective utilization of the in-house finite element software DENDRO.

REFERENCES

ABAQUS version 5.5 (1995) Hibbit, Karlsson and Sorensen, Inc., Pawtucket, RI, U.S.A.

Ballarini, R., Charalambides, P. G. and Islam, S. (1995) Near-tip dual length scale mechanics of mode-I cracking in laminated brittle matrix composites. *International Journal of Fracture* **70**, 275–304.

Bensoussan, A., Lions, J. and Papanicolaou, G. (1978) Asymptotic analysis of periodic structures. In *Studies in Mathematics and its Applications*, volume 5. North Holland, Amsterdam.

Charalambides, P. G. (1991) Steady-state mechanics of delamination cracking in laminate ceramic matrix composites. *Journal of the American Ceramics Society* **74,** 3066–3080.

Charalambides, P. G., Lund, J., Evans, A. G. and McMeeking, R. M. (1989) A test specimen for determining the fracture resistance of bimaterial interfaces. *Journal of Applied Mechanics* **56,** 77–82.

Charalambides, P. G., Zhang, W. and Ansari, M. M. (1995) Modeling of steady-state delamination in brittle matrix cross-ply composite laminates. *Journal of the American Ceramics Society* (submitted).

Christensen, R. M. (1991) *Mechanics of Composite Materials*. Kreiger, Malabar.

Clements, D. L. (1971) A crack between dissimilar anisotropic media. *International Journal of Engineering Science* **9,** 257–265.

Dundurs, J. (1969) Edge bonded dissimilar orthogonal elastic wedges under normal and shear loading. *Journal of Applied Mechanics* **36,** 650–652.

England, A. H. (1965) A crack between dissimilar media. *Journal of Applied Mechanics* **32,** 400–402.

Erdogan, F. (1963) Stress distribution in a nonhomogeneous elastic plane with cracks. *Journal of Applied Mechanics* **30,** 232–236.

Erdogan, F. (1965) Stress distribution in bonded dissimilar materials with cracks. *Journal of Applied Mechanics* **32,** 403–410.

Hutchinson, J. W. and Suo, Z. (1992) Mixed mode cracking of layered materials. *Advances in Applied Mechanics* **29,** 63–191.

Jha, M. and Charalambides, P. G. (1997) Crack-tip micro mechanical fields in layered elastic composites: crack perpendicular to the interfaces. *Int. J. Fracture* (submitted).

Jha, M., Charalambides, P. G. and Ballarini, R. (1997) Near-tip mode-I elastic fields in bimaterial layered systems. *International Journal of Solids and Structures* **34,** 1849–1871.

Lekhnitskii, S. G. (1963) *Theory of Elasticity of an Anisotropic Body*. Holden-Day, San Francisco.

Matos, P. P. L., McMeeking, R. M., Charalambides, P. G. and Drory, M. D. (1989) A method for calculating stress intensities in bimaterial fracture. *International Journal of Fracture* **40,** 235–254.

Muskhelishvili, N. I. (1953) *Some Basic Problems of the Mathematical Theory of Elasticity*. P. Noordhoff Ltd., Groningen, Holland.

Parks, D. M. (1974) A stiffness derivative finite element technique for determination of crack-tip stress intensity factor. *International Journal of Fracture* **10**(4), 487–504.

Qu, J. and Bassani, J. L. (1989) Cracks on bimaterial and bicrystal interfaces. *Journal of the Mechanics and Physics of Solids* **37,** 417–433.

Qu, J. and Bassani, J. L. (1993) Interfacial fracture mechanics for anisotropic bimaterials. *Journal of Applied Mechanics* **60,** 422–431.

Rice, J. R. (1988) Elastic fracture mechanics concepts for interfacial cracks. *Journal of Applied Mechanics* **55,** 98–103.

Rice, J. R. and Sih, G. C. (1965) Plane problems of cracks in dissimilar media. *Journal of Applied Mechanics* **32,** 418–423.

Sanchez-Palencia, E. (1980) *Non-homogeneous Media and Vibration Theory*. Lecture notes in physics, Springer, Berlin.

Shaw, M. C., Marshall, D. B. and Dadkhan, M. S. (1993) Cracking and damage mechanics in ceramic/metal multilayers. *Acta Metallica Materiala* **41,** 3311.

Sih, G. C., Paris, P. C. and Irwin, H. (1965) On cracks in rectilinearly anisotropic bodies. *International Journal of Fracture Mechanics* **1,** 189–203.

Tewary, V. K., Wagoner, R. H. and Hirth, J. P. (1989) Elastic Green's function for a composite solid with a planar interface. *Journal of Material Research* **4,** 113–136.

Ting, T. C. (1986) Explicit solution and invariance of the singularities at an interface crack in anisotropic composites. *International Journal of Solids and Structures* **22,** 965–983.

Williams, M. L. (1959) The stress around a fault or crack in dissimilar media. *Bulletin of the Seismological Society of America* **49,** 199–204.

Willis, J. R. (1971) Fracture mechanics of interfacial cracks. *Journal of the Mechanics and Physics of Solids* **19,** 353–368.

Zhang, W. (1994) Delamination studies of ceramic matrix composite laminates. Ph.D. thesis, Michigan Technological University.